Title
Cold Spray of Copper onto Niobium for Conductive Cooling of Superconducting Radio Frequency Structures

Author
Penney, James Kedren

Publication Date
2020

Peer reviewed|Thesis/dissertation

UNIVERSITY OF CALIFORNIA

Los Angeles

Cold Spray of Copper onto Niobium for Conductive Cooling of Superconducting Radio Frequency Structures

A thesis submitted in partial satisfaction of the requirements for the degree

Master of Science in Materials Science and Engineering

by

James Kedren Penney

2020

ABSTRACT OF THE THESIS

Cold Spray of Copper onto Niobium
for Conductive Cooling of
Superconducting Radio Frequency Structures

by

James Kedren Penney
Master of Science in Materials Science and Engineering
University of California, Los Angeles, 2020
Professor Jenn-Ming Yang, Chair

Niobium is used in superconducting radio frequency (SRF) structures that operate at cryogenic temperatures. These structures are continually optimized to increase efficiency and provide cost effective fabrication. Throughout optimization, material properties of thermal conductivity and mechanical strength are often jeopardized. Cold spraying has been of interest in coatings, repair, and additive manufacturing and poses a possible solution to optimization of SRF structures. This process involves deposition of a desired material onto a substrate through accelerating the material in the form of a powder to high velocities via pressurized gas. Currently, the combination of copper powder being deposited onto a niobium substrate via this process has never been studied. This is the first known study of cold-sprayed copper coatings onto niobium for the application of conductive cooling of SRF accelerating structures. Trials were conducted to assess the compatibility of cold spray of copper with SRF structures through processing and operating conditions. The material campaign involved understanding parameters for sample fabrication, substrate preparation, material deposition, and post-processing that may provide optimal coatings. This study offers a firm base understanding of the copper and niobium cold spray pair. Effective deposition of this pair requires mechanical interlocking as there is no metallurgical bonding of these materials at the processing temperatures. The extent of mechanical interlocking is affected by substrate preparation and surface roughness, oxygen content of copper powder, particle velocity, gas temperature, powder morphology, and particle size distribution.

The thesis of James Penney is approved.

Ya-Hong Xie

Jaime Marian

Jenn-Ming Yang, Committee Chair

University of California, Los Angeles

2020

DEDICATION

This thesis is dedicated to my mother and father who instilled in me a work ethic and set of values. To my big sister who continuously expands my world view. To Stefanie Polderman for making me feel as if you were by my side while you were a thousand miles away, your love and laughter drown out the world.

You should enjoy the little detours to the fullest. Because that's where you'll find the things more important than what you want. – Ging Freecs (Yoshihiro Togashi)

Contents

List of Figures

List of Tables

ACKNOWLEDGEMENTS

This thesis would not be possible without the support of my family, friends, and mentors. I appreciate each and every one of you for all your support.

A special thank you goes to those who have given me particular motivation and support throughout my growth as a scientist and engineer. My first Professor Dr. Ali Aliev for taking me into his lab as an undergraduate. My mentors KZ Inoue, Raquel Ovalle-Robles, and Chi Huynh for cultivating my creativity. My undergraduate institution, The University of Texas At Dallas for providing me a firm foundation. My good friend Angel Romero for reminding me there is always someone more intelligent. My mentor Dr. Paul Carriere for taking the time to guide me through my graduate career on the side of actually being my direct supervisor, thank you for your consistent insight and humor. My Professor Dr. Sergey Prikhodko for his patience, genuine attitude, and refreshing perspective as we waded through multiple projects that are completely unrelated to this thesis, meeting and working with you has been a pleasure.

We would like to acknowledge the entire Inovati team for their dedicated support during these cold spray tests, namely Ralph Tapphorn and Howard Gabel for their high level oversight, Travis Crowe and Jared Lettow for their on-site support, and Bryan Cyr for his programming efforts. We would also like to acknowledge the support provided by Chris Ledford and Tim Horn at NCSU, specifically regarding the donation of powder as well as supporting the LECO oxygen measurements. We are thankful to Dr. Ric Kaner and Dr. Chris Turner from the Department of Chemistry, University of California Los Angeles (UCLA) for use of the micro hardness measurement capabilities. Finally, we would like to acknowledge Professor Sergey Prikhodko from the Department of Materials Science, UCLA for his continuous support from the Electron Microscopy Lab and use of his facilities.

I would also like to include acknowledgement of RadiaBeam Technologies, my place of work during my graduate program, for being supportive of my goals and allowing me to be a part of their story. The work of this thesis is done through RadiaBeam. Lastly, thank you to the COVID-19 pandemic of 2020 for ensuring I had enough time to write this thesis.

1 Introduction

1.1 Motivation

Superconducting linear accelerators are in a growing demand in research and industrial applications. Currently, these devices are exclusively made from niobium, and advances in the art have been driven largely by new recipes to process the niobium surface, making the accelerators more efficient and cost effective. Unfortunately, these improvements come at the expense of other material properties, such as mechanical strength and thermal conductivity. The ability to make multi-material accelerators, while preserving the superior superconducting properties of niobium, is a topic of significant interest. Cold spray is a relatively new metallurgical coating process which can potentially solve this material optimization problem. Cold spray involves accelerating metal powder in a stream of gas to very high speeds and then impacting a solid substrate. The impact is so severe that the oxide layers normally separating the metals is broken or completely pushed out, resulting in a strong metal-to-metal bond. Cold spray is unique in that the powder is deposited without melting, which should minimize the risk of contaminating the niobium surface. This project will conduct the first-known study of cold-sprayed copper coatings onto niobium for superconducting RF accelerator components. The objective is to assess the compatibility of cold- spray copper with accepted SRF processing recipes and operating conditions. Some known risk factors, such as coating delamination, will be investigated experimentally in order to determine the feasibility of the cold spray approach towards SRF components fabrication. Multi-material SRF accelerating structures could significantly reduce the infrastructure required to operate these devices and reduce cost of ownership for the research and industrial accelerator systems. This would simplify the technology and expedite its adaptation by industrial applications.

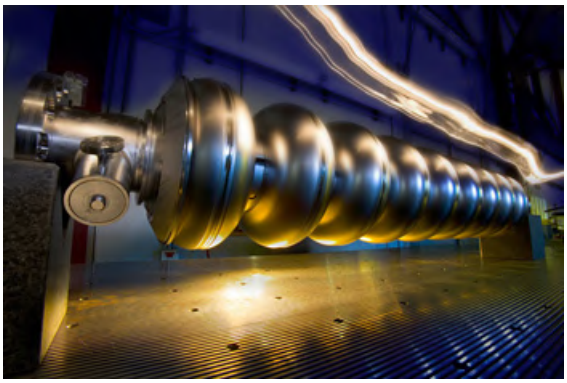

Figure 1: Example of Nb SRF Structure [Fermilab (FNAL)]

A real-world application is seen in the proposed International Linear Collider which, if built, will be the

longest linear particle accelerator, 10 times longer than the Stanford Linear Accelerator. In this design, superconducting radio frequency cavities, like the cavities seen in Figure 1, will be used as the main linacs for a length of 11km. Actively cooling this length of SRF structures requires a significant amount of infrastructure. Any optimization is magnified to make a large difference in design and cost at this scale.

1.2 Super Conducting Structures

Superconducting resonate frequency (SRF) structures are used in many applications from medical, industrial, and security purposes on top of the aforementioned large research linear accelerators. SRF structures are often made of niobium (Nb) and it is helpful to know the basics of SRF technology to understand the benefit of this study. The reason Nb is chosen for super-conducting cavities is due it's high transition temperature ($T_c = 9.3$K), high critical magnetic field ($H_c = 200$mT), being chemically inert, having the ability to be machined and deep drawn, and having availability as bulk/sheet material [1]. SRF structures only require a working surface of 45nm, the remainder of the structure serves solely as structural support. Additionally, for these structures to work properly, they operate in the range of 1.6-4.5 Kelvin. During operation, the cavities generate small amounts of heat on the surface which needs to be extracted at cryogenic temperatures. However, at this very low operating temperature the superconducting Nb has a low thermal conductivity. To initially overcome these areas of mechanical stability and thermal conductivity, the Nb structures utilize 3mm thick walls and the material used is triple refined via electron beam melting for the highest purity. This allows for a satisfactory level of mechanical stability and optimal thermal conduction without the use of multi-materials.

Despite being superconductive, very small amounts of heat are generated on the inner RF surface. If left unchecked, this heat will build up, leading to an increase in temperature and thus an increase in beam losses. This generated heat needs to be extracted from the inner surface through the niobium to an external heat transfer medium. This medium is often superfluid helium (He), which has incredible heat transfer properties but requires a large cryoplant infrastructure to work. A cryoplant is a system designed for active cooling of the structures down to cryogenic temperatures. These are bulky and costly to both install and operate. Cooling involves significant amounts of cryogen, e.g. helium, and the integration of multiple complex components such as heat exchangers, cryogen storage units, compressors, piping, purification systems, expansion engines or turbines, amongst multiple others [2]. Systems like these demand substantial space, energy, labor, and money to operate. Reducing any of these factors for industrial and laboratory applications has a direct impact on over \$500B/yr in products [3]. Achieving cryogenic temperatures is possible through another method called conductive cooling. Conductive cooling involves using a solid heat

transfer method to extract generated RF heat and reach desired temperature. Conductive cooling allows for a more cost-effective method and a more compact system. Reducing the individual accelerator cost and occupied space enables use for new applications and aids in overall simplicity [4].

To effectively apply conductive cooling, multiple materials other than that of the cavity can be employed. Many areas are explored here and one area with particular focus recently involves coating Nb cavities with a Nb_3Sn intermetallic through physical vapor deposition. This coating has a higher transition temperature than Nb alone and enables lower loss. This multi-material structure shows reductions in operational power [5] and thus promotes the use of conductive cooling with a simplified cryogenic system that does not require any gas or liquid cryogen [3]. Copper is a common choice to act as the material for conduction cooling. Specifically pulse tube cryocoolers suffer from issues with low efficiency due to poor radial thermal conduction. It is shown that the addition of copper plates to the structure significantly reduces the temperature deviations and improves efficiency [6]. This also goes for aluminum in some studies and the reduction of contact resistance for these techniques remains a goal for the cryocooler system [7]. A study on applying aluminum strips to conductively cool SRF cavities shows a compact SRF accelerator of dimensions 2x2x5 m^3 [8]. The cavity of this compact structure is shown as a thermal model in Figure 2 and reveals that the thermal contact resistance should be improved in order to successfully implement conduction cooling. Thus, routes are being explored to create a better bond that increases thermal efficiency of the coating material. Many SRF structures are also designed with mechanical stability in mind. Mechanical factors consist of stresses, vibrations, and Lorentz forces that can be taken into consideration through ellipticity, wall thickness, addition of stiffeners, and addition of static and feedforward dampers [9]. Cold spray offers a means of optimizing each one of these objectives using multi-materials. So far, the conduction cooling applications mentioned have attached any material acting as a heat sink through clamping or bolting [10, 8]. Applying cold spray to add copper to the Nb can potentially add a thermal conduction layer as well as a mechanical support layer onto the structure, while still preserving the purity of that 45nm layer.

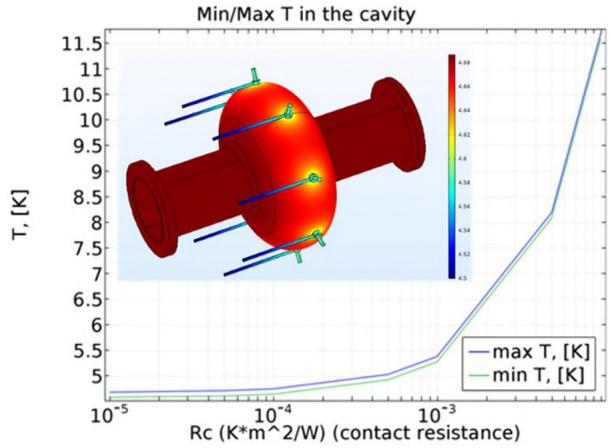

Figure 2: Conductive cooling: Cavity temperature vs thermal contact resistance between the cavity surface and AL rods [8]

As these structures reach operating temperature, their material properties change. The transition temperature of materials has been mentioned previously as well as thermal conductivity at operating temperatures. The transition temperature of a material is the critical temperature (T_c) at which a material below T_c exhibits superconducting characteristics. This is seen in the Nb and Cu that this study is focused around. To give an idea of how the scale of operation changes due to temperature, the Argonne National Lab calculates the difference in skin depth and surface resistance of Cu and Nb at different temperatures. The magnitude of the differences are seen in Figure 3 where Nb has a change in conductivity of 6-orders upon transition compared to Cu which experiences only 1-order. Something that also changes with temperature is the Carnot efficiency, which reaches 1.6% at 4.2K [11]. Increasing this efficiency can be done through lowering contact resistance and increasing conduction. Cold gas dynamic spray of Cu onto the Nb structure can potentially create a low contact resistance and uniform efficient thermal conduction for SRF cavities.

Skin Depth and Surface Resistance at 1.0 GHz			
T		Cu	Nb
293 K	Skin Depth	2.1 μm	6.1 μm
	Surface Resistance	8.2e-3 Ω/m^2	23e-3 Ω/m^2
~30 K	Skin Depth	0.2 μm	1.7 μm
	Surface Resistance	7.9e-4 Ω/m^2	6.3e-3 Ω/m^2
4.2 K	Penetration Depth	0.2 μm	0.05 μm
	Surface Resistance	7.9e-4 Ω/m^2	3.2e-7 Ω/m^2
2 K	Penetration Depth	0.2 μm	0.05 μm
	Surface Resistance	7.9e-4 Ω/m^2	6.5e-9 Ω/m^2

Figure 3: Behavior of Cu and Nb under different conditions and temperatures [11]

2 Literature Review

Presented in the following sections is a review of cold spray technology from mechanisms to design considerations. Also presented in this section are discussions on materials in this study and their compatibility for use as a cold spray pair.

2.1 Cold Spray Technology

Cold gas dynamic spray, or what we will call cold spray (CS), is considered *cold* because the process is solid state and the temperatures involved of the powder and gas are not high enough to cause any phase changes and melting is not required at the interface of the two materials for bonding to occur. This is significantly different than the deposition method of thermal spraying which involves a high temperature gas jet to accelerate heated/melted particles towards the substrate. The high processing temperature of thermal spraying results in local heating, oxidation, thermal deformation, phase transformations, structural changes, and hardening of both the coating and substrate with potential appearance of porosity and microcracks in the coating. Specifically, thermal spraying methods cause substantial changes of the material to which the coating is applied, such as electrical and heat conductance of the substrate, changes in the material structure from the chemical and thermal effects and hardening of overheated metals form the high temperature plasma jet, as well as ineffective powder particle acceleration (50-350m/s) due to the low density of the plasma [12]. As the material properties of the Nb cavity are essential to be maintained in this application, thermal spraying is not a viable option due to the disadvantages previously mentioned. The cold spray process consists of a metal powder, often in the range of 5-100μm, being shot at a chosen substrate. The metal powder is accelerated to velocities varying roughly 300-1200 meters/second via a pressurized gas stream to form a deposit or coating anywhere from 10μm to 50mm or more depending on the application [13]. These velocities ensure the thermal changes associated with thermal spraying are avoided. One method very similar to the cold spray process that also avoids these thermal changes and is considered a solid-state process is explosion cladding (EC). Explosion cladding introduces a shock pressure that promotes bonding through a "surface jetting" effect, the same jetting effect that is a main feature in cold spray bonding. The main difference between these two joining processes is the impact velocity of the particles. EC estimates impact velocities of 1400 to 3900m/s compared to cold spray velocities of 300-1600m/s implying the jetting effect is less intense in cold spray [12]. At these velocities, EC and cold spray both allow for the joining of materials with significant differences in melting temperatures without any need for an intermetallic. As the range of impact velocities is different, cold spray also allows for precision control of powder particle velocity, enabling control of the structure and properties of the

deposited coating.

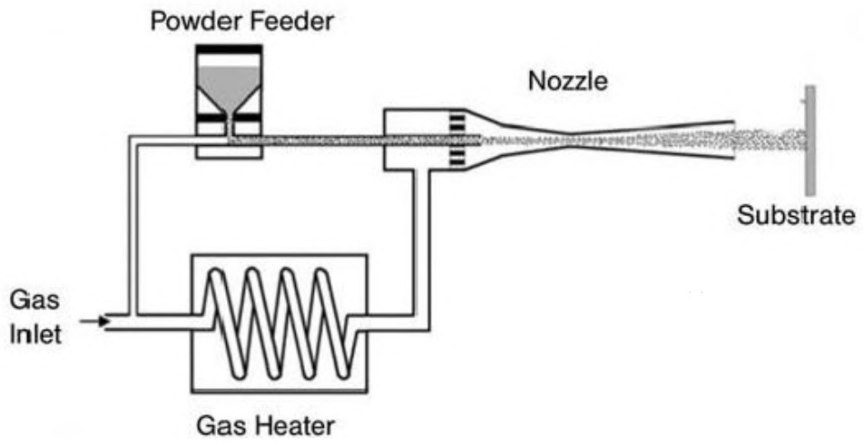

Figure 4: Layout of traditional cold spray setup [14]

The velocity of the powder depends on the accelerating gas velocity. The gas exit velocity is dependent on gas pressure, gas temperature, and nozzle design. The gas stream can be denoted as high pressure or low pressure. High pressure cold spray is used to describe supersonic velocities achieved by high pressure gas (up to 30 bar = 3MPa or 435psi) preheated (up to 1000°C) to optimize aerodynamics. The preheated high pressure gas is mixed with the powder before being fed into a converging-diverging 'DeLaval' nozzle which results in accelerated particles with sufficient kinetic energy to impact the substrate and induce bonding (600-1200 m/s). Low pressure is used to describe subsonic velocities (300-600 m/s) achieved by preheated gas (up to 10 bar and 550°C) in which powder is fed into the nozzle by the Venturi effect. The low pressure system can be safer, more portable, cheaper, have longer service life, and accepts modifications easier than high pressure systems but is unable to achieve similar deposition efficiency as high pressure systems [15]. The differences in the spray setup can be seen in Figure 5. The main differences here are the location the powder is introduced to the flow and the pressure ranges. Accelerating gas consists of either helium, nitrogen, a mixture of these two, or dry air. High pressure often uses helium while low pressure often uses air or nitrogen. Helium allows for higher velocity to be achieved but has the downfall of being costly, while nitrogen does not allow for as high velocities but is cost effective. This leads to many combinations for design purposes. As a new material and substrate are being developed, it can be a quick check on the sprayability of the two materials by depositing with high pressure helium. If there is no adhesion of the powder at this process parameter, it can suggest the two materials are not an optimal cold spray pair. It is not always possible to optimize and eliminate the use of helium. This is not a downfall of the technology as the cold spray process can still lead to much more effective results compared to other deposition/coating processes.

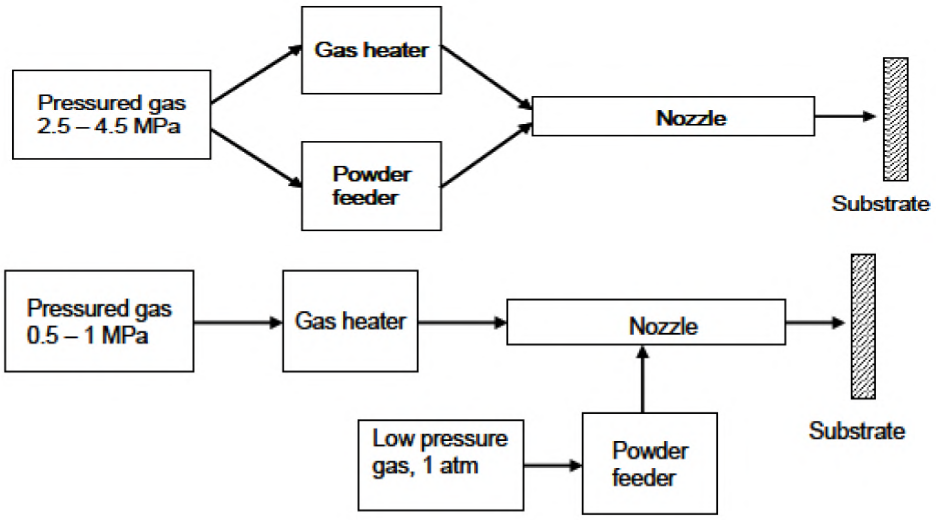

Figure 5: Differences between Top: High Pressure CS and Bottom: Low Pressure CS [13]

Kinetic Metallization (KM) is a term for the application of spraying with subsonic gas velocities, not traditional low pressure cold spray, made possible with a specific nozzle design. The process used in this study in particular is KM with a patented process created by Inovati [16]. KM focuses on maximizing particle velocity while maintaining gas density. Maintaining gas density as close to Mach 1 as possible allows for a longer dwell time for particle acceleration, resulting in particle velocities similar to or exceeding the more common supersonic spray methods while using 1/10th of the pressure. Less gas pressure is much more cost effective as gas consumption, specifically helium, is a concern with high pressure CS methods. South Dakota School of Mines and Technology (SDSMT) has a good introduction to the gas dynamics of cold spray deposition [17]. This report by SDSMT presents similar information that is discussed below on how gas pressure, composition, flow, temperature, standoff distance, powder size and material all affect deposition characteristics. Figure 6 shows an introduction of gas dynamics through a converging-diverging nozzle. The gas flowing through this nozzle undergoes pressure changes which result in the gas having different velocity and temperature from the start of the nozzle feedthrough until impact with the substrate.

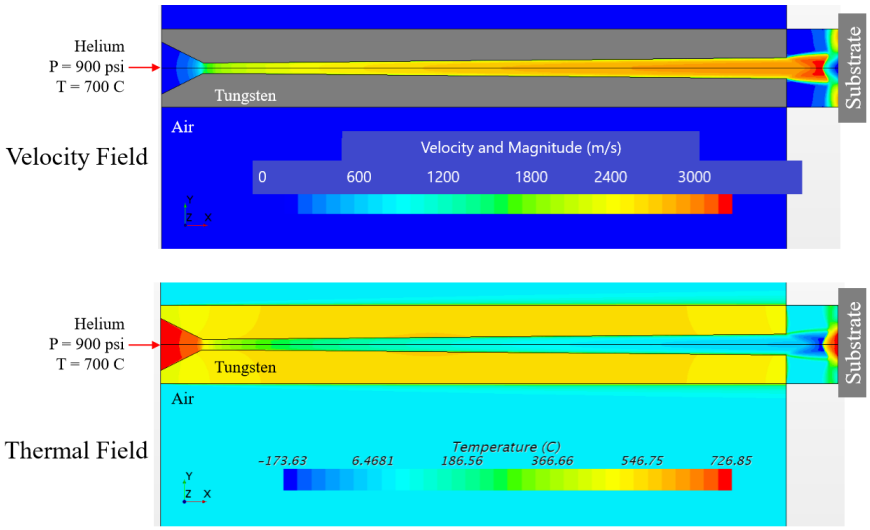

Figure 6: Gas dynamics through a de Laval nozzle showing the velocity and temperature through the spray process [17]

The deposition that occurs through the cold spray process can be explained by a combination of two bonding methods. The first is mechanical interlocking of the powder and the substrate due to deformation upon impact, this is a physical bond. Mechanical interlocking is explained in Figure 7 where higher pressures allow for an increase of 'mixing' at the coating/substrate interface. The second is a metallurgical bond of the coating/substrate interface, this is a chemical bond. These processes can be aided through substrate preparation. The substrate can be polished, ground, grit blast, high pressure water rinsed, etched, and can undergo multiple other processes in order to promote bonding of a particular material pair.

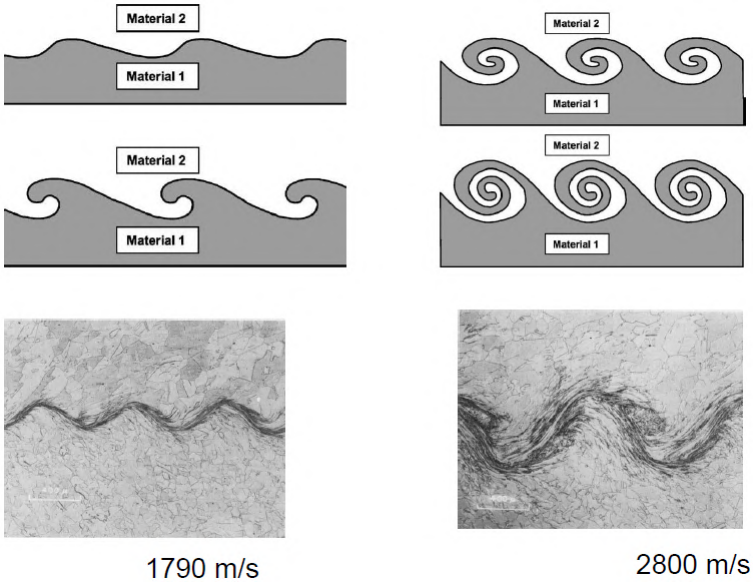

Figure 7: Bond zones of nickel clad on nickel made at different collision velocities showing effect of mechanical interlocking [14]

The initial layer of deposition is critical to good adhesion and thus the substrate preparation and spray parameters are optimized for this layer. A key process in the initial layer is the removal of any surface oxides. An increasing oxide layer thickness has been shown to decrease particle deformation and thus impacts adhesion. Trying to minimize the oxide layer via surface preparation before the initial layer or removing the oxide layer during the initial spray is important. This oxide layer can effect both metallurgical and mechanical bonding. The impact of the initial layer has been studied and suggests there is a high strain rate deformation process during particle impact resulting in an adiabatic shear instability creating a metal jet [18]. The creation of this metal jet composed of particle and substrate is the proposed reason for removal of the surface oxides [19]. The substrate preparation and particle velocity both have an impact on the efficiency of surface oxide removal during initial layer deposition. For effective adhesion to the substrate, the particle must be at or above what is considered a critical velocity. A particle at critical velocity is what creates the crater and metal jet discussed, best seen in Figure 8 with images corresponding to different velocities. The particle velocity is controlled with the gas pressure and is impacted by the powder morphology. If the gas velocity is below the critical velocity, the powder does not have enough kinetic energy to plastically deform and bond to the substrate. If the gas velocity is above the erosion velocity, the incident particle will have excessive kinetic energy resulting in substrate erosion without deposition. Between these two extremes lies the window of deposition [20].

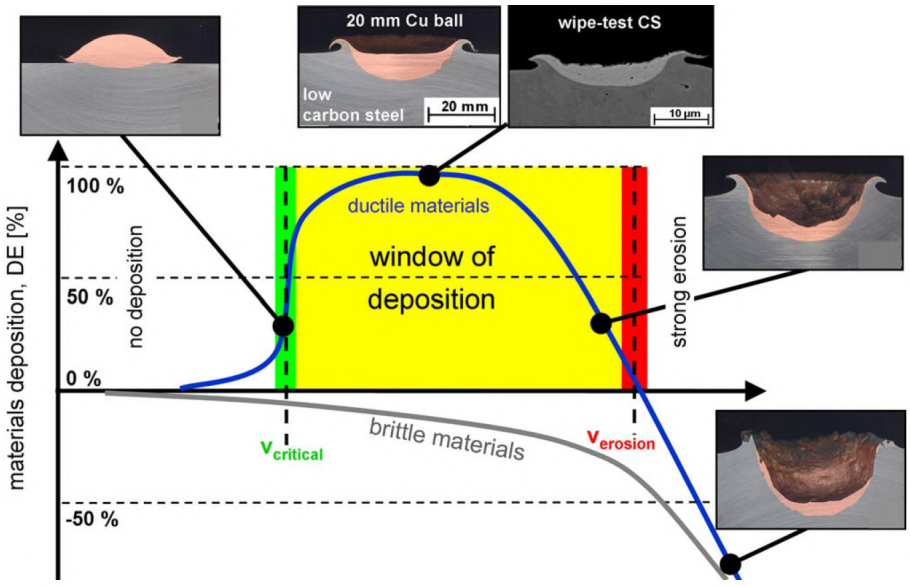

Figure 8: Powder splat characteristics in relation to velocity depicting a window of deposition [20, 21]

After this initial interfacial coating, the following deposition layers require particle-particle bonding of the powder material impacting previously deposited layers and still rely on a window of deposition. Powder

within the window of deposition implies good deposition efficiency, low porosity, and well-adhered coatings. Deposition efficiency is a ratio of the weight of particles adhered to the substrate to the total weight of the particles sprayed in the coating process. This is a measurement that is useful in determining the effectiveness of spray parameters. Increasing the deposition efficiency generally correlates to more optimized parameters, also useful for large scale processes where powder needs to be used efficiently for cost considerations. Porosity is a measure of the coating itself as a ratio of volume of voids with the total volume of the coating. This can be measured using destructive 2-D cross section microscopy combined with image analysis or non-destructively with more precision using a gas pycnometer or X-ray tomography. Porosity is important for properties of the coating whether mechanical, thermal, or electrical. One factor in decreasing porosity is the compressive force of additional layers depositing on previously sprayed material. Adhesion is another useful measurement for comparing spray parameters and is used as a qualitative and quantitative test. It is possible to have a well adhered initial layer and still have high porosity or a low deposition efficiency.

During the particle-particle-substrate bonding, the powder and substrate undergo significant deformation. This can generate some unwanted results in the materials. If the substrate is grit blasted in order to promote bonding, this can cause work hardening which in turn limits the deformation of the impact which can result in less effective removal of surface oxides and/or a lower bond strength [19]. The same process of work hardening that can occur in grit blasting the substrate occurs in the sprayed particles. As deposition occurs, the particles undergo severe plastic deformation and this results in residual stress build up and heat generation. As the spray process is often linear, residual stress can build up in one direction and cause delamination during the spray process. While the magnitude of residual stress in cold spray is less than that of thermal spray coating, it can still be detrimental to the mechanical stability and functional performance of the coating [22]. The high velocities and pressures in cold spray generate predominantly compressive residual stresses. These stresses have been found to be caused by a combination of three main factors which are particle density and deformation behaviour, difference of the CTE of the coating material and substrate, and temperature, velocity and critical velocity of particles [23]. There are currently methods to measure and mitigate the amount of residual stress build up during cold spray and the development of these techniques is ongoing. This residual stress may not be an issue for some processes, but is important to keep in mind for others that require extreme environments that encounter rapid cooling or heating.

In addition to strictly focusing on velocity, the gas can be heated to increase gas velocity and allow the powder to more easily deform with more energy on impact. The temperature of the gas can be anywhere between 25-350°C [14], with some high pressure systems applying temperatures up to 900°C. Particle

temperature plays a role in the bonding process as well. It is reported that increasing particle impact temperature significantly decreases the critical velocity of copper [24]. Lowering the critical velocity can be done by increasing gas temperature, enabling lower gas pressure which can be cost effective. Figure 9 presents this relationship of powder temperature and critical velocity. The powder particle energy, consisting of thermal and kinetic energy rather than only kinetic energy as particle velocity, has a direct result on the deposition characteristics. Understanding the amount of energy that comes from this thermal energy during the spray process is difficult to define exactly as it consists of a complex relationship between gas temperature, specific heat of the gas and powder material, time of exposure, and nozzle type. Gas is also noted to react with changes of density and viscosity at different temperatures, which will have a direct impact on deposition. Thus this area is still being fully defined and parameters are often based on what has worked for other spray pairs or experiments and expanded from there. This synergistic relationship of gas temperature and pressure is an example of how cold spray can still rely on trial and error for some variables despite a significant amount of research in any particular powder/substrate combination [25].

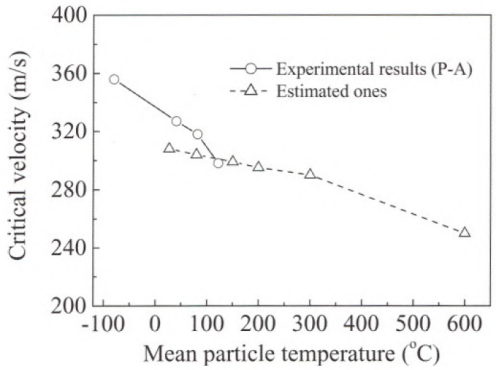

Figure 9: The effect of particle temperature on critical velocity of powder deposition depicting a higher particle temperature resulting in a lower critical velocity [15]

A topic that is not discussed often is the tamping effect. This occurs during the particle-particle bonding phase where the newly sprayed layers compress the layers below. The tamping effect can be seen at the substrate interface on a micrograph. During the coating process, two layers are formed. The first is a layer in the coating that stands out as more severely compressed than the remainder of the coating. The second is a less compact layer that lies above the first layer. The bottom layer is created through the tamping effect and this layer is seen to have significantly less porosity than the top layer [26, 14, 27]. Looking out for the tamping effect in micrographs can reveal a lot of information on the deposition characteristics. Figure 10 is a diagram of a micrograph where stage 1 is the initial substrate preparation and interfacial layer, stage 2 is the bulk deposition, Stage 3 shows a reduction in porosity and compaction of the previously sprayed layers, and stage 4 shows is excess kinetic energy resulting in cracking and

unwanted deformation.

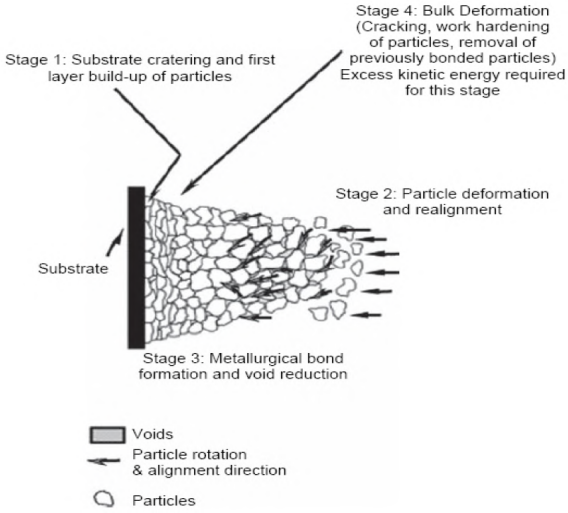

Figure 10: The 4 Stages of Cold Spray including Stage 3: Compaction i.e. 'Tamping Effect' [15]

2.1.1 Atomization

The powders that are used for CS are primarily created through an atomization process. Atomization is a fascinating technique that allows for creation of elemental or alloyed powders with a large size distribution and specified morphology. Atomization is a process in which liquid metal is ejected through a nozzle at a turbulent flow to cause separation into small droplets and quickly cooled by inert gas or water. The jet flows directly into a large closed chamber that can also have an inert gas or water jet spraying at the opening to increase turbulent flow and further formation of droplets. This chamber is important to minimize immediate oxidation of powders and to cool the powder effectively. The nozzle diameter, velocity of liquid metal, and cooling ability are some of the factors that determine the morphology, size distribution, porosity, and overall efficiency [28].

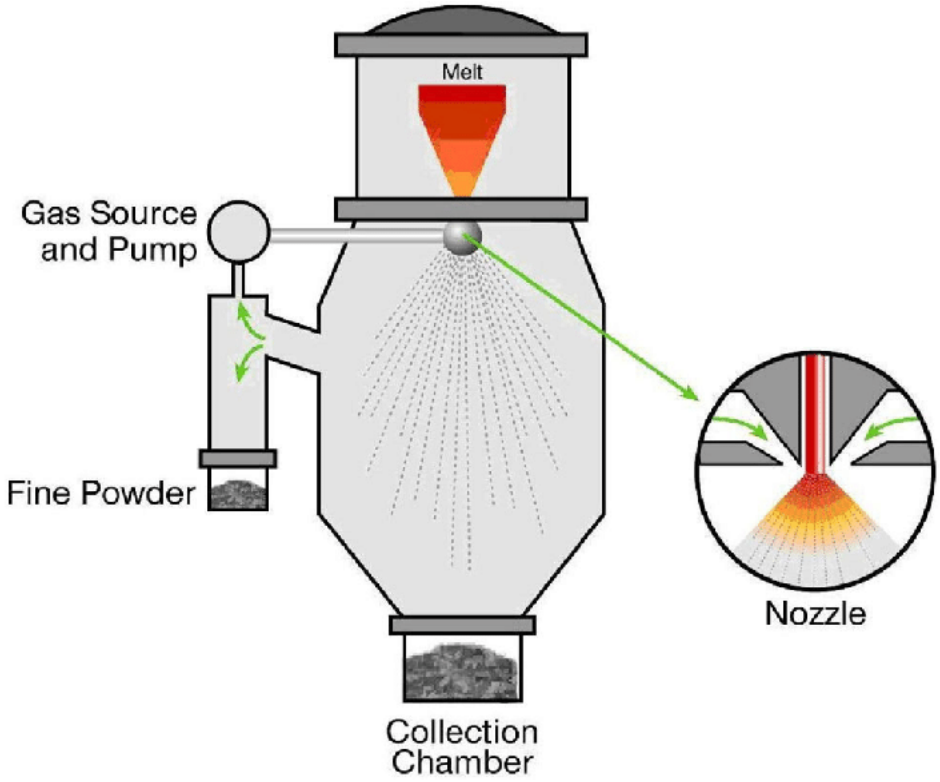

Figure 11: Gas Atomization [28]

This process does not allow for precise control over size distribution of powders so the powders are either immediately sorted into more concise size distributions in the chamber via gravity or cyclonic filtration or they are sorted post-process as needed. One example of powder size distribution being important is in cold spray repair processes where a fine size distribution aids in higher density of deposition layers. This is also seen in additive manufacturing via powder metallurgy where the powder size distribution affects the spreadability. The powders that do not fit within this applicable size distribution are sieved out and set aside for later use. A problem arises when there is no found use for a large majority of sieved powders that are either too large or too small. This is not a large issue for many applications but it goes to show that while atomization is established and impressive, there are always places for development.

2.1.2 Design Considerations

Specific applications of cold spray have not been mentioned. Cold spray can be used for the spray of similar metals and repair damaged or corroded parts to as-new performance. The deposition assists in improved heat transfer, electrical conductivity, and enhanced corrosion and wear resistance. Cold spray is especially useful when the substrate and deposited layer are not compatible with methods such as thermal

spraying or explosion bonding. When looking at a cold spray pair, there is more to consider than just a critical velocity for a given powder and substrate material. One factor that has not been presented is powder morphology and particle size distribution. Powder morphology refers to the powder having a spherical or amorphous shape. These are described as spherical powder (SP) such as the tungsten powder in Figure 12 and irregular powder (IP).

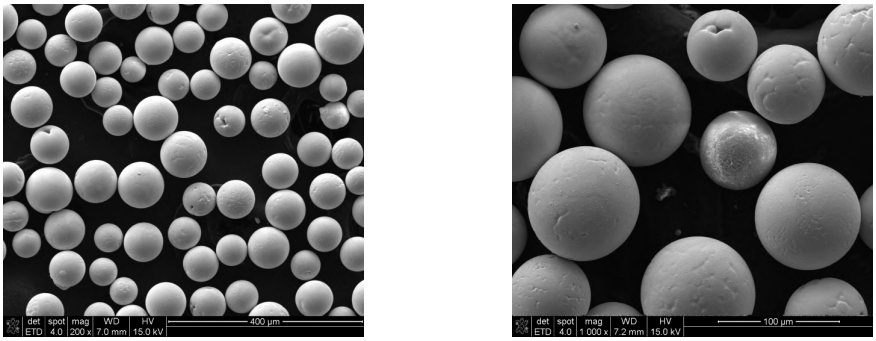

Figure 12: SEM of spherical (SP) tungsten powder

The particle size distribution refers to the amount of powder in terms of size, for example whether the powder consists of primarily 25μm or a full range of 5-120μm. The particle velocity is partially dependent on powder morphology, among other parameters, which has subsequent effects on the deposition efficiency, porosity, and extent of the tamping effect. A study at McGill University on cold spray of Ti splats on sapphire suggest that the adhesion of SP is less dependent on particle velocity than IP [27]. IP has a higher particle velocity to reach before significant adhesion is achieved compared to SP. This is an insight to design considerations in regard to morphology. The splat dynamics, contact angle, jetting upon particle impact are all explored in this referenced study of Ti/Sapphire.

As the particle size distribution effects spray results, cold spray processes often used sieved powder with a tighter particle size distribution. Knowing the particle size distribution is one step towards finding your particle velocity and thus your critical velocity. This is seen in the charts of Figure 13, a larger particle size results in a lower particle velocity and a smaller particle size results in a higher particle velocity under certain spray conditions.

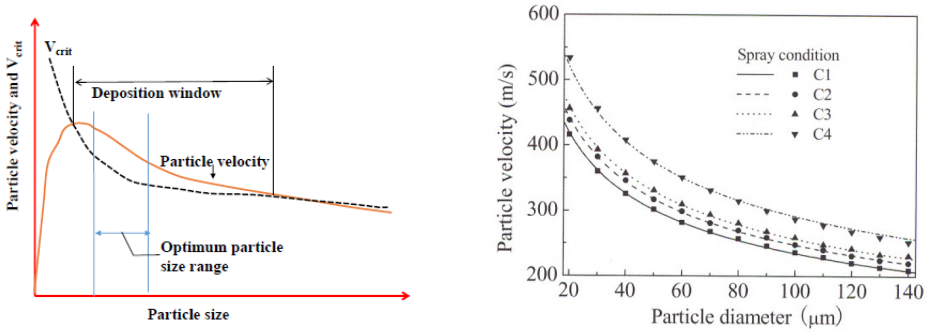

Figure 13: Particle velocity dependence on particle diameter for a given spray parameter with Left: deposition window and critical velocity shown and Right: relation of decrease particle diameter resulting in increased velocity [14, 15]

The pressure, temperature and composition of the gas, particle velocity, deposition energy, powder morphology, and particle size distribution have been discussed. There are multiple other criteria that need to be recognized. The first set of criteria involves the actual cold spray setup. A particular cold spray setup will have a specific nozzle design that cannot be changed, be it high pressure or low pressure, etc. The parameters of a CS setup that can be changed are the powder feed rate, nozzle travel speed, standoff distance, incidence angle, spray environment, and coating deposition rate. The powder feed rate is the amount of powder, in grams, that is fed through the gun per a unit of time. The travel speed is the speed at which the nozzle moves depositing the powder. The standoff distance is the distance from the substrate surface and the nozzle head, this is often in a fixed range for each particular nozzle but sometimes is the small change needed to cause a successful deposition. The incidence angle is the angle of the applied deposition. This angle is often perpendicular to the substrate for maximum deposition efficiency. Depositing onto complex geometries is an important ability for any CS setup and requires the ability to maintain the incidence angle and standoff distance on any object, a main reason for the setup being mounted onto a multi-axis robotic arm. One circumstance the incidence angle may change is if there is a problem with embedding of grit blasted particles. The desired coating can be sprayed at a large incidence angle of 45°+ in order to roughen the substrate surface without depositing any material or embedding unwanted material. The spray environment is whether the deposition is done in air or under inert gas. The deposition rate is a function of the feed rate and travel speed and determines the coating thickness of one spray pass.

After deciding the thickness of coating desired, finding a balance between powder feed rate and travel speed for the desired deposition rate is a calculation away. One needs to decide if multiple layers need to be deposited as well, i.e. number of spray gun passes required to reach desired coating thickness. Something to keep in mind is that as the deposition occurs, the substrate and coating heat up due to the incident

kinetic energy being transformed into thermal energy resulting in a stress build up in the direction of the deposition layers. The temperature of the surface after particle impact can increase as the travel speed decreases as seen in Figure 14, nozzle travel speed also impacts deposition efficiency and coating thickness so a balance between these factors is ideal. This stress build up may not cause any issue, but in certain cases the substrate can deform if thin enough or the coating can delaminate. In this study multiple layers of Cu were deposited on a copper plate for fabrication of RRR samples. The copper plate was only a few mm thick and bent arching upward due to this thermal stress. This thermal stress can always be removed with post process heat treatment if the coating does not delaminate during spray. If it is an issue during the spray process and other routes of improvement have been explored unsuccessfully, then consider decreasing the deposition rate and having more layers. It is also possible to increase gas pressure while reducing gas temperature. One unexplored route is a non-repeating non-linear travel path along the substrate to mitigate stress build up in any one direction. A study published in Surface & Coatings Technology took a theoretical approach to thermal stress build up of Ni on Ni. This shows a significant relationship between nozzle travel speed and the temperature and deposition characteristics. The most obvious being a faster travel speed resulting in a thinner deposition layer, and the most impactful being a faster travel speed resulting in a slower temperature buildup but a lower deposition efficiency. These are characteristics to keep in mind when developing a cold spray coating. This is one example of how having a thermocouple attached directly to the substrate during the spray process can offer necessary insight.

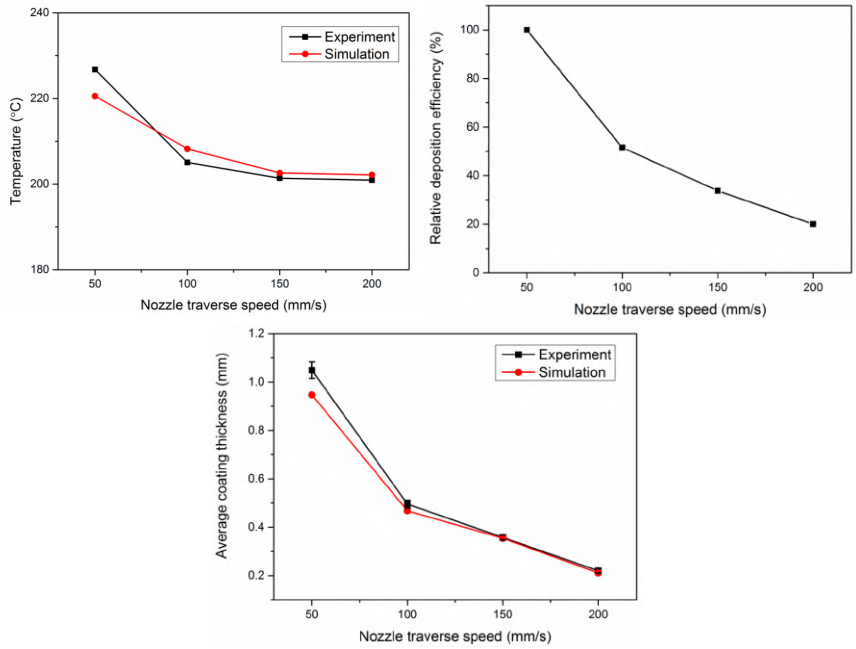

Figure 14: Nozzle travel speed effect on deposition characteristics with Top Left: Temperature; Top Right: Deposition efficiency; Bottom: Coating thickness [29]

The last criterion to recognize during a CS setup is the substrate preparation. Substrate preparation plays a large factor in successful adhesion and is always a question when looking at any CS process. This can be anything from a simple cleaning to grit blasting. Substrate preparation is critical to create a surface that promotes adhesion through ideal metallurgical bonding and mechanical interlocking. Adhesion is dependent on substrate morphology in the form of surface roughness, oxide layer, and hardness. The oxide layer has been discussed, and there are methods to remove this oxide layer such as chemically cleaning or oxidation heat treatment. The substrate hardness in relation to the spray material has a clear impact as the larger this hardness gap the less natural the deposition will be. This is partly why similar metals are so compatible with respect to cold spray, due to similar deformation characteristics. Similar metals in cold spray is more or less the same as those considered in welding. Similar metals possess similar chemical or mechanical properties while dissimilar metals possess different chemical or mechanical properties. This is a generic definition and some examples can help explain. An example of similar materials is Ti-6Al4V powder deposited onto Ti-6Al4V substrate while an example of dissimilar materials is the Ti/Sapphire mentioned previously. It is also possible that two metals, austenitic steels, can be welded together but still be different enough alloys to be considered dissimilar [30]. Factors that need to be considered when welding dissimilar metals are as follows: solubility, intermetallic compounds, weldability, thermal expansion, melting rates, corrosion, and end-service condition [30]. These welding considerations are not far from those looked at for cold spray. It is suggested that the deformability of the substrate decreases as the hardness increases and that particles have more difficulty bonding to a surface in relation to this decrease in deformability [31]. Grit blasting is often used in surface preparation to increase surface roughness, but should be noted that grit blasting can increase near surface microhardness of the substrate. An increase of surface roughness is found to cause an increase in deformation of particles and subsequently better adhesion from an increase of mechanical interlocking. Kumar [32] suggests that surface roughness with a crest/trough measurement similar to the particle size results in better bonding. This study by Kumar looks at hard-hard, soft-hard, and hard-soft powder-substrate combinations at varying surface roughness including comparing the contact time and rebound energy of the deposited particles. This shows how complex this parameter can be depending on the material spray compatibility. Below is a bar graph depicting CP-Ti onto Ti6Al4V in which grit blasting, increased surface roughness, actually has a negative impact on the quality of adhesion.

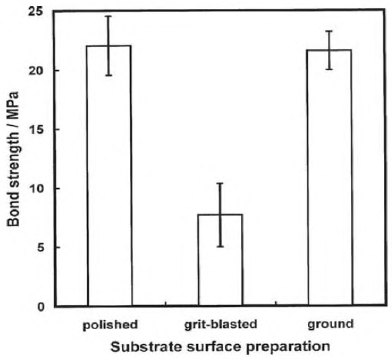

Figure 15: Effect of substrate condition on the bond strength of CP-Ti deposits sprayed on Ti6Al4V substrates [31]

In certain cases, grit blasting is not an acceptable practice due to substrate wall thickness, previous deposition, brittle substrates, and most importantly the surface contamination from particle embedding. Particle embedding from grit blasting is prevalent in soft substrate materials. One surface preparation technique utilizes a pulsed waterjet (PWJ), a waterjet with 69MPa pressure at 20Hz frequency from a 1mm nozzle diameter [33]. This has been studied for Al coatings by the Cold Spray Research Laboratory in Ontario and resulted in an increase of surface area and adhesion strength compared to grit-blasted and polished surfaces. The surface roughness can be controlled via standoff distance and the substrate has no embedded particles from grit blasting. Another alternative practice to grit blasting is based on the principle of 'delay time' of deposition. There occurs a brief time during the spray process between when particles make contact with the substrate and actual deposition begins. This time is considered the delay time in which the particles are roughening the substrate surface without adhering. This can be a technique utilized, similar to Figure 16 below, in which the powder is sprayed at a higher than normal velocity or 'erosion velocity' for a short period of time to activate the surface with increased surface roughness before reducing the velocity for desired deposition.

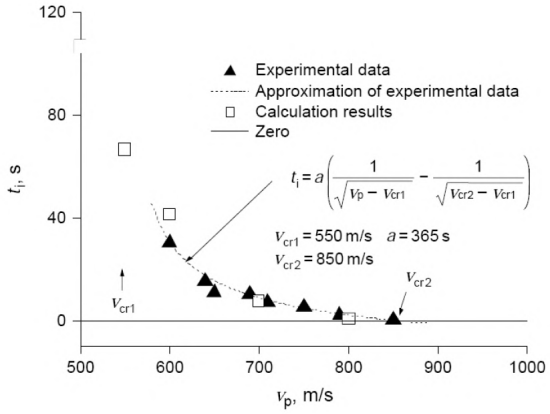

Figure 16: Deposition delay time versus the mean impact velocity of aluminum particles on a polished copper substrate [31]

In certain CS processes, the cold spray pair and the application do not allow for desired level of bonding. However, it is possible to add an interlayer between the two called a bondcoat. A bondcoat is any material thinly deposited as the initial layer on the substrate used to ensure adhesion. The desired coating is then deposited onto this bondcoat. Choosing a bondcoat depends on the application of the process as well as the materials. A bondcoat can be needed due to a lack of metallurgical bonding between the substrate and the coating as well as to aid in CTE mismatch.

Determining the process parameters of a CS setup is non-trivial. There are a lot of options and defining characteristics of a coating and determining all of these parameters can take trial and error. It is suggested to take the materials in question, equipment at hand, desired results, previous research, and all process parameters into consideration before commencing with deposition as doing so can expedite development.

2.2 Cu/Nb Compatability

Cold spray's most common applications come from Aerospace and repair of large structures and due to this Cu and Nb have not been studied as in-depth as some other materials such as Ti-64. This is currently the first in-depth study on Cu coating on Nb via cold spray for the application of SRF structures.

Cu and Nb have some challenges facing them as a cold spray pair. Firstly, they are dissimilar metals. CS is used often in repairs due to the spray material being the same as the substrate. A study attempting to model the CS process and identify the window of deposition and optimal velocity using what is called 'smoothed particle hydrodynamics' (SPH) found a relation between CS of similar and dissimilar materials metals [34]. This study used a measure of ratio between the particle velocity and rebound velocity, this ratio is called the coefficient of restitution. They go on to measure this also with rebound energy and deposition energy, taking into account temperature and particle size. The rebound energy is found as the

energy of a particle after impact, essentially the kinetic energy remaining from an elastic collision of the particle onto the substrate. A particle below critical velocity or above maximum velocity will have high rebound energy which results in no bonding to the substrate. Maximum velocity of a particular particle is defined as the velocity in which the rebound energy exceeds deposition energy to the extent that no adhesion occurs and the particle rebounds. A particle at optimal velocity will be considered to have a coefficient of zero. Applying this to multiple spray pairs and correlating to physical experiments shows that similar metal coatings are more easily deposited than dissimilar metal coatings. This is due to a large amount of initial kinetic energy being dissipated as plastic dissipation energy in similar metals. In dissimilar metals, there exists more rebound energy which leads to lower deposition efficiency and higher porosity. In the graph below, similar metals show a lower deposition and rebound energy ratio compared to dissimilar metals.

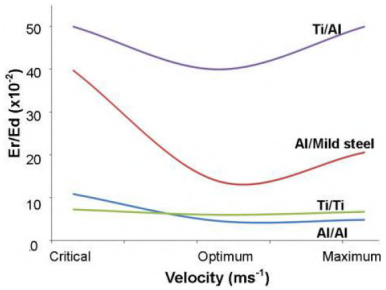

Figure 17: Comparison of deposition and rebound energy ratio between impact of similar and dissimilar metals [34]

According to general CS principles, copper and niobium form a 'sprayable' material pair, as both materials have low yield strength, are ductile, and do not form any brittle intermetallics [25]. Unfortunately, Cu and Nb have very limited solubility, extremely different melting temperatures (1083°C vs 2477°C), high interfacial surface energy/poor wetting and different crystal structures (Cu as FCC vs Nb as BCC) [35, 36]. The metallurgical compatibility of Cu/Nb has been mentioned multiple times. A good way to demonstrate this low compatibility is through a materials wetting characteristics and phase diagram. Looking at the phase diagram of Cu-Nb in Figure 18, no intermetallics form across the composition range. There is a peritectic reaction at 1090°C where the solubility of either material to the other does not exceed 1.6wt%. This temperature exceeds the melting temperature of Cu as well as any temperatures experienced throughout the entire spray process. There is negligible solubility of copper in niobium at ambient temperatures and less than 0.2% for niobium in copper. This information is from a study on depositing liquid copper onto solid niobium and found that wetting is low even at the peritectic temperature [36].

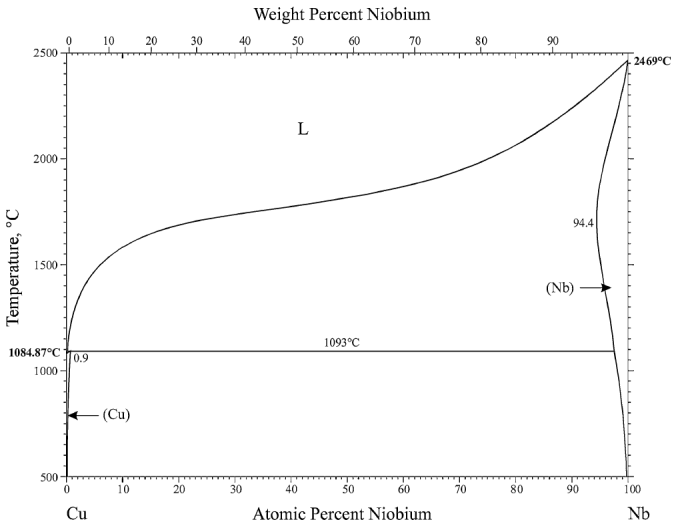

Figure 18: Copper and Niobium Phase Diagram [37]

Braze processes can give insight to the wetting of two materials. One quick experiment was done in house, at RadiaBeam, to demonstrate the difficulty overcoming the interfacial surface energy of Cu/Nb. Braze alloy CuSil, consisting of 28% Cu and 72% Ag, was placed on turned Nb coins and ran through a braze cycle that reaches 795°C, above the CuSil liquidus point of 780°C [38]. Figure 19 depicts the CuSil/Nb combination before and after braze without any wetting of the Nb substrate. While this is below the melting point of pure copper, it is well above the temperatures achieved in the cold spray process.

Figure 19: CuSil braze alloy Left: before braze cycle and Right: after braze cycle failed wetting of Niobium

The compatibility of Cu/Nb was explored further with a study at Sandia National Labs on diffusion bonding of Cu to Nb. Diffusion bonding was possible with specific parameters of surface preparation, furnace atmosphere, and bonding temperature, pressure, and time. Sandia studied diffusion bonding of Cu to Nb to act as interfaces for the application of joining ceramic faces. A braze alloy Nicoro + 2% Ti (35% Au, 62% Cu, and 3% Ni) was used to bond Nb to alumina and Cu to alumina individually. It was found that Cu can be bonded to Nb and that Nb will diffuse into Cu. This was carried out at less than half the melting temperature of Nb, 50°C below the melting temperature of Cu, and there were no voids at the

interface resulting in a metallurgical bond. No special surface preparation was performed and the samples were cleaned using basic degrease processes directly after being cut. However, Nb samples were annealed before the diffusion bonding process at 1400°C for 15 minutes with an average grain size of 16μm +/- 1μm [35]. Diffusion bonding is an especially interesting technique for studying materials compatibility, since the interface between materials is well defined, and the relevant thermodynamic and kinetic parameters are carefully controlled (time, temperature, pressure). In comparison, cold spray is a much more stochastic process, and is therefore more challenging to tease out competing phenomena. From these studies, it was found that strong metallurgical bonding could be obtained by diffusion bonding for 3hrs at 1050°C with 4.1MPa of pressure. When the bonding temperature was reduced to 1030°C, poor adhesion between the Nb and Cu was measured, with the differences of the interface morphology shown below.

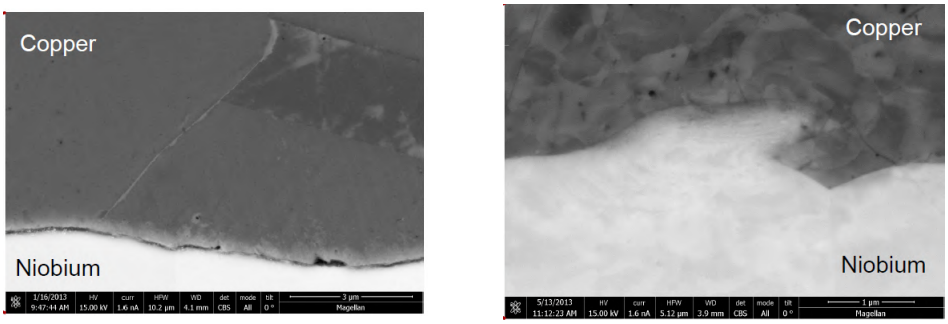

Figure 20: SEM cross sections of diffusion bonding of Cu/Nb at Sandia National Labs with Left: Poor Nb/Cu bonding using 1030°C/3hours/4.1MPa and Right: Cu-Nb interdiffusion using 1050°C/3 hours/4.1MPa [35]

Detailed transmission electron microscopy was used to demonstrate that Nb diffused approximately 5-6μm into Cu while no Cu diffuse into Nb. These process parameters are not compatible with this study. The temperatures involved during diffusion bonding are excessively high, which will result in excessive grain growth in the Nb and loss of mechanical strength. This reinforces the belief that in order to successfully deposit Cu powder onto Nb substrate, mechanical interlocking is key as there is no metallurgical bonding at these temperatures.

Interestingly, Cu and Nb can also form what is called an orientation relationship at their interface. Specifically they form the Kirjumov-Sachs relation in which the planes shown in the figure below are parallel at the interface of the two materials.

$$(111)_{fcc} || (-110)_{bcc}$$
$$[1\text{-}10]_{fcc} || [111]_{bcc}$$

Figure 21: Kurdjumov-Sachs relationship: copper and niobium orientation relationship [39]

This relationship is not taken into account for this cold spray study as it is a macro process. However,

future pursuit of Cu/Nb interfaces should be aware of this relationship during diffusion bonding, physical vapor deposition, accumulative roll bonding or some other process where the quality of interface at such a small scale is critical. This relationship at the interface can aid in mechanical and thermal properties through a reduction in defects as found through a study on Cu-Nb laminate composites by Los Alamos National Laboratory [39].

The coefficient of thermal expansion (CTE) of Cu/Nb is mismatched with Cu at 16.5x10$^{-6}\mu$m/m/K and Nb at 7.3x10$^{-6}\mu$m/m/K. This needs to be understood for both the cold spray process itself and future processing of the cold spray pair. This CTE mismatch could create unwanted thermal stress during heat treatment and cryogenic cooling [40]. Concerns regarding coating spallation due to differences in CTE could be problematic when one considers a standard SRF thermal cycle between vacuum hydrogen degassing (1073K) and cryogenic operation (<2K). Simplistic estimates of the residual stress due to the thermal expansion mismatch in a two-layer system can be described by the following equation [41]:

$$\sigma_c = \frac{1}{d_c}\left(\frac{\alpha_s - \alpha_c}{\frac{1-\nu_c}{d_c * E_c} + \frac{1-\nu_s}{d_S * E_s}}\right)\Delta T \tag{1}$$

Where σ, α, d, ν, and E are the thermal interface stress, coefficient of linear expansion (CTE), coating thickness, Poisson Ratio and Young's Modulus, respectively. In the above equation, the subscripts 'c' and 's' refer to the coating and substrate, while ΔT refers to the temperature difference of the coating process compared to the service temperature.

The key takeaway from Eq. 1 is that the large differences in CTE between Cu and Nb (σ_{Cu}=16μm/m°C versus α_{Nb}= 7μm/m°C) will increase interface stresses and promote coating spallation. Furthermore, temperature variable in Eq. 1 highlights the advantage of cold spray, as high temperatures are not needed to generate adhesion, thus reducing the as-deposited interface stress. This is further highlighted by applying the 'thin' coating limit (dc<<ds) while taking advantage of the similar Young's Modulus (115GPA/105GPa) and Poisson ratio (0.36/0.4) for Cu/Nb, which reduces Eq. 1 to:

$$\sigma_c = \frac{(\alpha_s - \alpha_c)E_c}{1 - \nu_c}\Delta T \tag{2}$$

In this case, we can explicitly see that the interfacial stress is directly related to the CTE mismatch between Cu and Nb. A requirement of this study is to provide sufficient adhesion in order to overcome the negative effects of CTE mismatch, at a minimum through initial deposition and processing if cold-shock experiments are not achieved. If sufficient adhesion is not achieved, understanding how this thermal induced stress can be mitigated for further downstream processing can be taken into design considerations.

This could be done through methods such as a more straightforward approach of increasing gas pressure and reducing gas temperature to less common approach of applying a non-linear spray pattern.

2.2.1 Copper as a Coating

Copper is the chosen material for this application of conductive cooling for the impressive thermal properties. Previous examples of SRF structures involving Nb and Cu are discussed in the Introduction, section 2.2. The properties of OFE Cu are displayed in the chart below. The percent of elongation is representative of the ductility of the material. Cu having high ductility and high thermal conductivity is ideal for this application as a sprayable coating as this results in a soft-hard powder-substrate combination that maximizes conduction cooling.

Table 1: Mechanical, thermal, and electrical properties of OFE Cu at 99.99% purity

Properties of OFE Cu	
Density	8.9 g/cc
Hardness Vickers	90
Tensile Strength Ult.	254 MPa
Tensile Strength Yield	78 MPa
Elongation at Break	55%
Modulus of Elasticity	117 GPa
Machinability	20%
Electrical Conductivity	101% IACS
Electrical Resistivity	0.00000168 ohm-cm
Thermal Conductivity	391 W/m-K
CTE	17.0 µm/m-°C
Melting Point	1083°C

(a) [MatWeb]

OFE Cu has a purity of 99.99% and 0.0005% oxygen. Cu powder in this study is created through atomization. During this process, the powder is not exposed to air. However, this changes as the powder is transferred from the atomization chamber to a storage unit. Cu forms a native oxide on it's surface at a slow rate at room temperature. This native oxide is only nanometers thick and oxides do not begin to diffuse past the surface until 150°C. This oxidation is magnified by the high surface area of metal powder. The surface area of 1 gram of Cu in the form of a cube (nearly 5x5x5mm) is 150mm^2 while the same 1 gram in the form of 25μm powder results in a surface area of 2,993mm^2. It is proven that the level of oxidation of Cu powder as a direct impact on the quality of deposition via an increased critical velocity required [42].

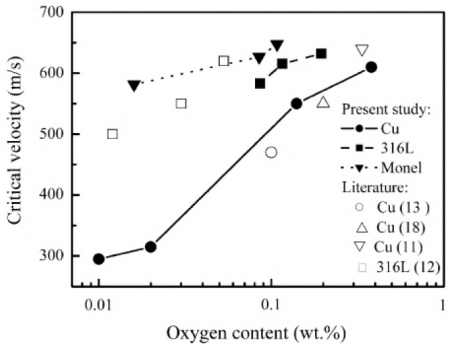

Figure 22: The effect of oxygen content of powder on the critical velocity [15]

The presence of surface oxides in Cu powder results in oxide inclusions during the spray process. As the powder collides with either the surface or previous layers, the oxide layer surrounding the powder breaks. A large portion is removed during the jetting that occurs in deposition while small oxide inclusions have been found remain in some scenarios. This directly effects the adhesion strength as more inclusions decrease adhesion strength.

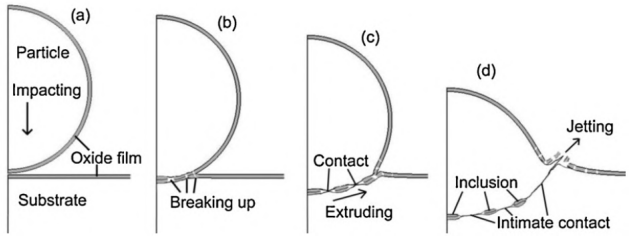

Figure 23: Diagram of formation of oxide inclusion during material deposition and jetting process [42]

A study at the University of Brussels summarized the optimisation of Cu cold spray [43]. They found that the particle velocity (a summation of multiple spray conditions and particle size distribution) and the oxide content are the main important factors that influence the deposition efficiency. A thesis published by the Naval Postgraduate School looked at microcrystalline and nanocrystalline copper and copper alloys desposited via cold spray. They were able to find that coating thickness per pass, spray temperature, and spray pressure are important levers in adjusting deposition efficiency. One particular note from this study that is not often mentioned is the role of excess temperature. As deposition occurs, excess temperature can cause residual stress when cooling which can degrade bond strength or even full delamination from the substrate [44]. This should be kept in mind when thicker coatings are necessary and an increase of pressure can be more favorable than an increase in temperature.

2.2.2 Niobium as a Substrate

Nb is chosen as the substrate material because of it's superconducting properties. The properties of Nb are different depending on the purity. This purity can be characterized by the residual resistivity ratio (RRR) and commercial Nb can be considered to have a RRR value less than 100 and higher purity Nb will have a RRR value of roughly 300. A brief insight to mechanical properties of commercial Nb is shown in the table on the left of Figure 24a. The material used in this study is high RRR Nb, specifically RRR of 300. RRR values are related to the SRF performance of the cavity but to achieve these high RRR values the properties related to formability and mechanical behavior once formed must also be balanced. It is important to distinguish amongst these properties of Nb and it is a give and take in finding the optimal combination of properties for the application. Some of the mechanical properties also differ with purity. Firstly, properties of Young's modulus (E_{273K} = 104.9 GPa and E_{2K} = 126.5 GPa) and Poisson's Ratio (v = 0.397) are intrinsic of Niobium [45]. The intrinsic properties introduced are related to the mechanical resistance, or stiffness, of the material, along with the Yield Strength and Elastic Limit. Nb can have high purity but poor formability, seen in Figure 24b. The Yield Strength is around 35-70 MPa for Nb that has been well processed and annealed while it can be well over 100 for high RRR Nb with poor formability. The percent of elongation is representative of the ductility of the material and is seen to be much higher in high purity Nb.

Cryocoolers undergo significant temperature differentials and vibrations through testing and operations and are already pushing the limits of mechanical stability in these regards. The Elastic Limit changes with temperature as well. This limit is higher as grain size decreases and the effect of twinning becomes apparent in Figure 25 showing a significant decrease with reduction/elimination of twinning. The mechanical issues mentioned thus far can be shown further in the thin walls of Figure 26 depicting a weld between two half cells. These walls are thin to allow for sufficient thermal efficiency of the system. All of these properties are related through forming to assembly and result in the substrate of this cold spray application. Based on these properties and comparing to Cu, Nb and Cu form a soft-hard spray combination. According to Kumar [32], this soft-hard spray combination has an advantage over other combinations in an increased contact time. This combination is not as similar to more common soft-hard pairs such as Al on steel due to the high ductility of the Nb allowing for more deformability of the substrate. One thing to keep in mind during any soft-hard spray combination is that the powder is not as easily able to cause plastic deformation of the substrate, thus mechanical surface preparation might be necessary. The very short time-scale thermo-mechanical response of Nb during coating is also studied by Kumar in [24].

Properties of Wrought Nb	
Density	8.6 g/cc
Hardness Vickers	160
Tensile Strength Ult.	585 Mpa
Tensile Strength Yield	78 MPa
Elongation at Break	5%
Modulus of Elasticity	103 GPa
Electrical Resistivity	0.0000151 ohm-cm
Thermal Conductivity	54.4 W/m-K
CTE	7.10 µm/m-°C
Melting Point	2468°C

(a) Properties of wrought Nb with low purity

Mechanical properties [a] \Batch	A	B
Yield Strength $\sigma_{0.2}$(MPa)	66	150
Tensile Strength σ_m(MPa)	180	183
Elongation A (%)[b]	59	40
Strain Hardening Coef. n [c]	0.31	0.10
Hardness Hv	56	65
Grain size (ASTM)		
- core	6	5
- surface	6	6
Formability	GOOD	BAD

(b) Properties of high purity Nb with good and bad formability

Figure 24: Mechanical properties of (a) low purity Nb and (b) high purity Nb [45]

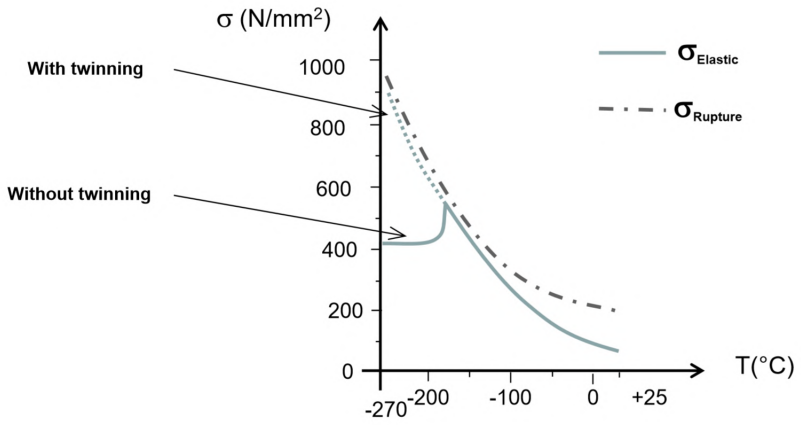

Figure 25: Elastic limit of ultrapure Niobium with and without twinning while varying temperature [45]

Past the mechanical properties of the bulk Nb, the surface properties of the formed cavity are also important. A study by Argonne on the braze of Nb to stainless steel (SS) with a Cu filler utilized a buffer chemical polish (BCP) of 1:1:2 hydrofluoric, nitric, and phosphoric acid. The Nb part was etched for 3 minutes with a priority to etch less than 24 hours before the planned braze cycle [38]. This further reinforces the premise that BCP is necessary to prepare the Nb surface for any process, such as brazing or cold spray, and the timeline of surface preparation and intended processing is important. This surface preparation serves to remove contamination and surface oxides. Another common practice is high pressure rinsing shortly before processing or braze to remove any contamination in the form of organic and inorganic residue. The surface oxides on Nb build up rather quickly during the first 24 hours of exposure to air to reach a thickness of 25Å before the rate decreases significantly [46]. A larger concern than surface oxides and contaminants is hydrogen ingress of Nb. Niobium is known to develop hydrogen ingress through initial processing and/or environmental conditions. Niobium hydrides form at the surface and contribute to the degradation of the superconducting properties in cavities [45].

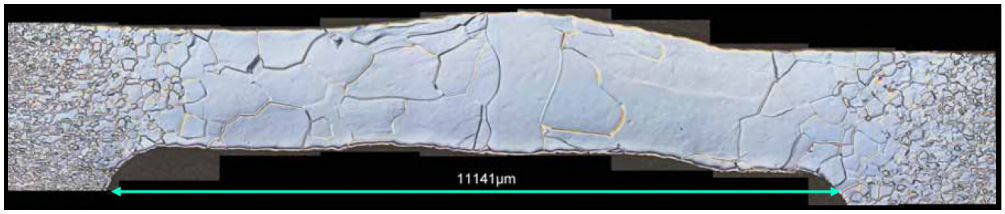

Figure 26: Cross section of weld between two SRF Nb half cells connected by E-beam welding [1]

There are two reasons Nb structures often undergo high vacuum annealing at temperatures up to 800°C. The first is for degassing to mitigate issues of hydrogen ingress. Argonne finds that hydrogen degassing begins at temperatures as low as 400°C. Their standard process for their Half-Wave Resonator Cryomodule is high vacuum annealing of the large Nb structures at 650°C for 10-20 hours, while others apply the annealing at 800°C for 2 hours. This results in a spike of hydrogen partial pressure which decreases by orders of magnitude through the degassing process. The hydrogen partial pressure appears to dominate the gas load during vacuum bake-out, this precision requires a fully dialed-in and leak-tested vacuum system. This can be utilized for rough understanding of any changes of pressure seen in our in-house vacuum furnace during vacuum annealing as no partial-pressures are available. A short etching (less than 5 m) is needed to eliminate diffusion layers of oxygen and carbon after high vacuum annealing. However, the Niobium will have hydrogen ingress again after several months of room humidity. Cracking of Nb from oxygen and hydrogen diffusion is studied at high temperatures at University of Florida, Gainesville revealing further the reason to mitigate the introduction of these gases [47].

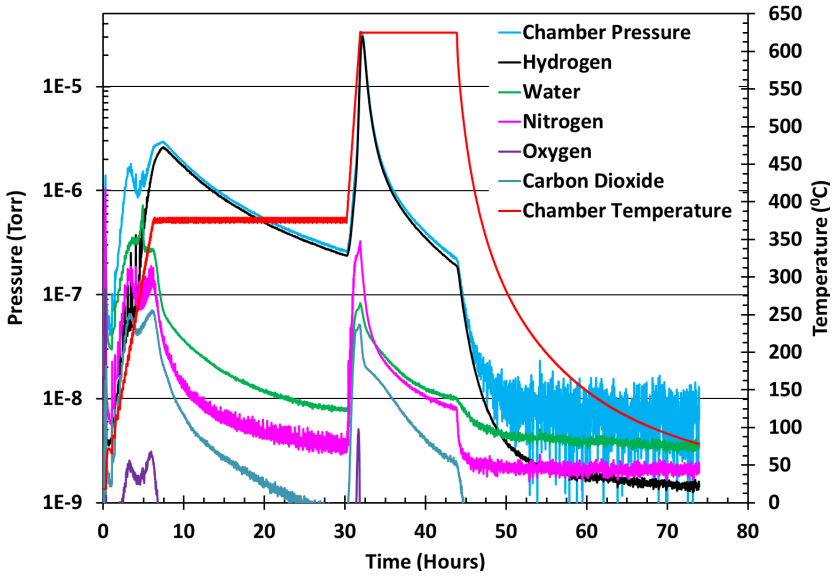

Figure 27: Vacuum Annealing: Hydrogen degassing over time at Fermi National Accelerator LaboratoryL [11]

The second reason for high vacuum annealing is for the recrystallization or recovery of Nb. The

recrystallization temperatures decrease with increasing purity such that commercial Nb temperature ranges from 900-1000°C, 800°C for RRR of 300, and 750°C for RRR above 400 [45]. Annealing cavities at or above these temperatures acts as a 'reset' to erase cold working of former processing steps. Recovery and recrystallization mostly occur at the same temperature but recovery can be obtained without recrystallization using a lower temperature, slow annealing rate, long duration, or argon quenching. High vacuum annealing allows for recovery which decreases dislocation density and for removal of hydrogen contamination. These process steps and their purpose can be see in Figure 28 from Claire Antoine [45].

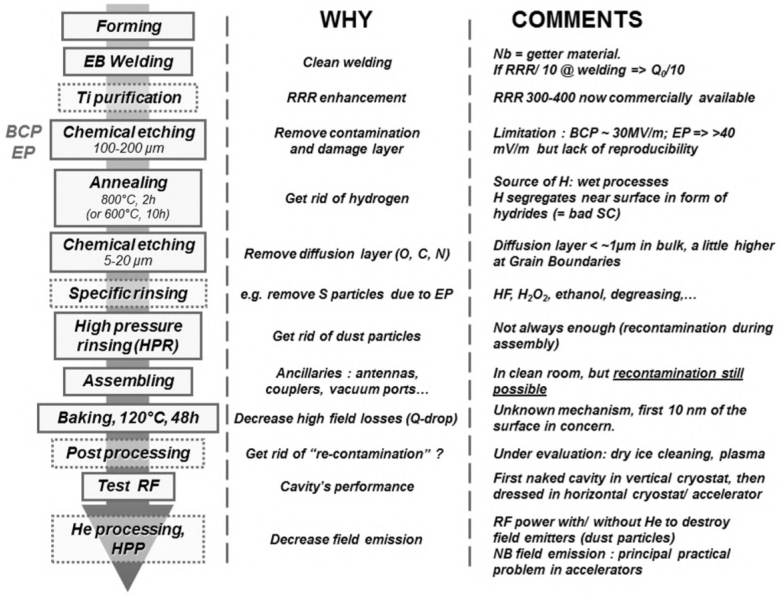

Figure 28: Stages of preparation of superconducting cavities. [45]

The difference between commercial Nb and RRR 300 Nb is significant. The processes and forming necessary to achieve high RRR cavities also effects mechanical and thermal properties. The Nb substrate used in this study attempts to replicate these properties such that the cold spray deposition of Cu and the thermal properties of the sprayed samples behave as would be expected of a fully processed SRF Nb cavity.

2.2.3 A Word About RRR

Residual-resistivity Ratio (RRR) is an important variable when looking at the two materials. RRR is a ratio of the resistivity of a material at room temperature and at 0K. However, due to 0K being impossible to reach, temperatures such as 2K are used for measurements in practice. This is seen in Eq. 1 where ρ represents thermal conductivity. An understanding of RRR is required to understand this study, mainly this aides in understanding the motivation of prioritizing the minimization of oxygen content in deposited powder. RRR is known to be dependent on scattering by impurities such as dislocations and oxygen

content, so minimizing oxygen content on top of a quality coating with good adhesion and minimal porosity suggest a higher RRR value. Figure 29 depicts the RRR of Nb is able to significantly increase as the gas concentration of oxygen decreases to 10ppm. At the moment, RRR values could prove to be a testing standard for this application. However, there have been no RRR measurements of as-sprayed Cu or annealed Cu cold spray for this study. This is interesting to measure as the Cu behavior at lower temperatures has a significant impact on the efficiency of the cryocooler.

$$RRR = \frac{\rho(295K)}{\rho(2K)} \tag{3}$$

Fabrication of the Nb structures begins with high RRR Nb sheets to achieve the best outcome of material properties throughout the process. The RRR begins at 300 and the final structure undergoes some heat treatment to results in a RRR value of 300-500. Starting with optimal material properties is not applicable for atomized Cu powder and the only controlled parameters can be minimization of oxygen pickup throughout the cold spray process post atomization. The dependence of RRR in relation to impurities is shown in the chart below. This depicts the presence of oxygen playing a larger role in RRR value than other chemical impurities of gas concentration.

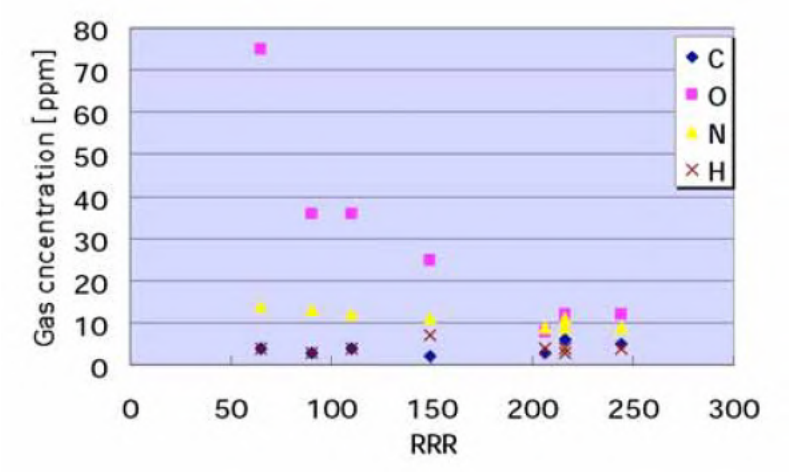

Figure 29: RRR of Nb vs gas concentration [4]

A sample of cold spray was created for the use in RRR measurement to be conducted at Jefferson Labs. The samples were prepared with a substrate of OFE Cu as a rectangle of 7x10 cm and 4 mm height. The substrate was coated with the same Cu powder used in the remainder of the experiment, discussed in materials and methods, at a thickness of 4 mm. JLab requested samples of 2x2x50mm so the deposited layer was machined to the required dimensions. One sample was then heat treated similar to the treatment given to the Cu/Nb samples and sent to JLab for RRR and thermal conductivity measurement. The

samples were to be placed in a setup similar to the one seen in Figure 30-b. However, the experiments were not carried out and the effort was abandoned due to scheduling.

(a) RRR Samples- Top: non-heat treated, Bottom: heat treated

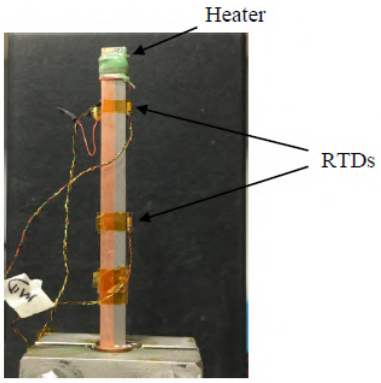

(b) Setup for thermal conductivity measurements at JLab

Figure 30: Samples to be tested at Jefferson Labs for RRR and Thermal Conductivity

The performance of copper at these temperatures is more important in this study. As the Nb used will be processed to it's best properties, the newly introduced Cu coating has to perform well.

Ordinary copper:	5<RRR<150
OFHC copper:	100<RRR<200
Very pure copper	200<RRR<5000

Figure 31: Expected RRR values of various oxygen content and purity of Cu [48]

Copper that is cast normally is shown to have reasonably high RRR. Specifically the most often used material is oxygen free high conductivity (OFHC) Cu that has RRR in the range of 100-200. This would be a desired range of RRR of the Cu cold spray coating if measured. At the same time, some studies have been done on alternative methods of Cu coating. RRR of electroplated Cu 30 microns thick is studied at the Laboratory of the Linear Accelerator (LAL) in France and finds a RRR of around 20. This value is increased by a factor of 6 (from 20 to 120) when subject to one hour of 400°C vacuum annealing [49]. LAL performed a custom setup for electrical conductivity measurements at a temperature range of 4.2K - 300K and used this data to convert to an estimated RRR value. This data correlated to other findings well. A similar approach is used to correlate electrical conductivity through eddy current measurements to thermal conductivity in this study, however no such in-house low temperature measurements were performed. These findings suggest that reducing impurities and defects, reducing oxygen concentration, and annealing the Cu are all helpful in maximizing the RRR value of the Cu coating.

3 Materials and Methods

A description of the equipment used as well as some processes deemed significant are listed below. One thing to note is that this study involved only two separate rounds of spraying separated by a few months. Each round has some unique differences and will be referenced as first and second round of spraying, with the second round being performed with some additional insight from the results of the first.

3.1 Cold Spray Equipment

Inovati was a partner on this study. All CS equipment was used at their facilities in Santa Barbara, CA. Inovati has a custom patented spray technology, Kinetic Metallization (KM) [16]. KM utilizes a nozzle design that allows for particle velocities similar to those reached during high pressure cold spray but at significantly lower gas pressures. This is done so by maintaining gas density past the nozzle exit. Gas density decreases at supersonic velocity past the nozzle throat, this in-turn decreases it's ability to push particles. Maintaining gas density as close to Mach 1 as possible allows for a longer dwell time for particle acceleration, resulting in particle velocities similar to or exceeding supersonic spray methods while using 1/10th the pressure. Lower gas pressure means less gas used, which is extremely cost effective for the use of helium. The spray booth is designed for this method and allows for safe powder handling and adaptive deposition processes. The spray nozzle is attached to a robotic arm with 6-axis movement. Parameters that the hardware/software are able to control are feedrate, travel speed, standoff distance, gas temperature, and gas pressure.

(a) Spray booth at Inovati

(b) Chamber

Figure 32: Spray booth of Inovati equipment

The spray booth was modified for spraying of the Nb samples during the second round. The chamber is usually continuously venting and pulling powder out of the chamber during the spray process to minimize powder build up and possible health and safety hazards. During deposition of the Cu layer, the vent was turned off and covered and the spray booth was purged with Argon gas throughout the spray. The Argon gas filling the booth was measured with an O2 sensor and the spray began once the O2 sensor read below 2%. The purpose was to minimize oxidation of the samples during the spray process as the temperature of the surface and speed of deposition caused visible oxidation of samples without this procedure.

Figure 33: Oxygen sensor after Argon purge of chamber for deposition; Reading 1.5%

The 6-axis motion is not often needed for it's full potential. In this study, we sprayed a non-conformance Nb half cell that is used for cryocoolers that this study designed for. Inovati was able to take a CAD rendering of the cell into their software and design a spray path customized for the unique shape. The cell is a complex rounded shape approximately 8" in diameter with a steep curvature that includes overhangs. The capability to spray complex shapes is a critical design feature for this application.

Figure 34: Approximately 8" Diameter: Nb SRF Cell used for a CAD rendering to enable Inovati to create a custom spray path

3.2 Pre-Spray Preparation

The niobium used during these trials was parted from a 30mm diameter, 800mm rod procured from ULVAC, Japan. The material chemistry met standards for ASTM B393 Type 5, corresponding to a RRR > 300. Nb buttons were parted with a thickness of 3mm. 8x Nb buttons for Round 2 were then turned on a lathe with the intention to achieve a higher surface roughness than as-parted surfaces. The Nb samples were then cleaned ultrasonically in hot Citranox and rinsed with AR-grade isopropyl alcohol at RadiaBeam. This process was performed for both Round 1 and Round 2. Of the button coupons having 30mm diameter and 3mm thickness, 11 Nb coupons were prepared in Round 1 and 12 Nb coupons were prepared in Round 2.

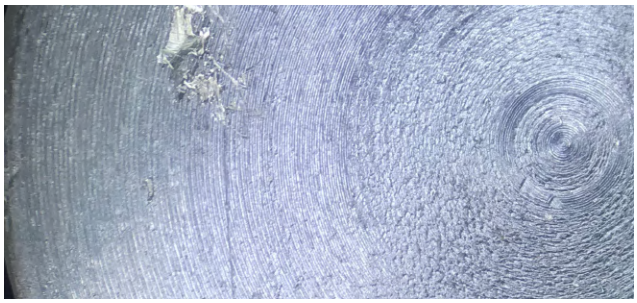

Figure 35: Image of Surface Profile of Turned Nb in Round 2 Samples - Scale is 15mm from the circular center to edge

Round 1 coupons were grit blasted without any additional surface preparation before being sprayed

with Cu powder. Round 2 underwent additional processing in efforts to eliminate the step of grit-blasting. The processing was buffer chemical polishing (BCP) of 8 as-turned Nb samples and 4 samples that had been roughly ground with 120 grit SiC paper. BCP etching was performed using the standard 1:1:2 HF:Nitric:Phosphoric composition (discussed in Section 3.2.2) immersed in an ice bath. The ice bath is important to control etch rate as the solution is not temperature controlled, the etch rate will exponentially increase along with the temperature if it is not controlled. Some additional handling, safety, and waste management protocols were developed to perform this operation. BCP etching is performed to completely remove any oxides or contamination on the surface so that bonding is promoted with an ideal surface.

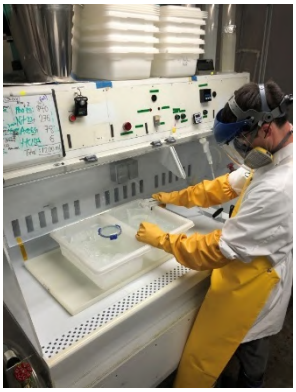

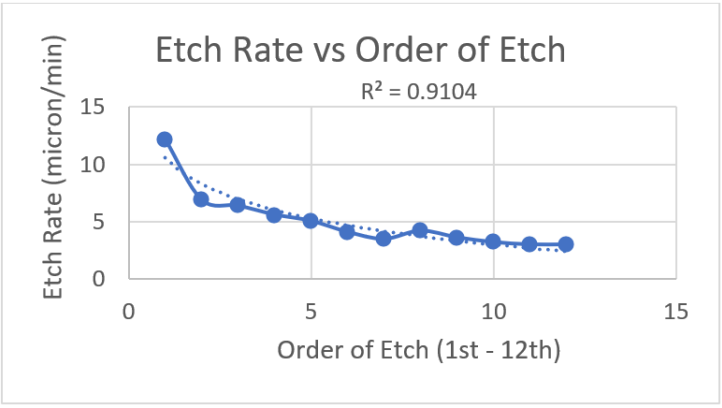

Figure 36: Left: BCP of Nb in ice bath Right: Etch rate decline with increase of Nb content

BCP etching shows a significant drop in etch rate as the active etching species, HF and NO_3, are depleted. However, this does not effect the quality of the etch for our purposes as sufficient exposure time can overcome this depletion. Any possible contaminations and oxide layer have been removed when subject to this BCP for 2 minutes. 2 minutes of BCP exposure corresponds to approximately 10 microns of uniform material removal for the standard surface area of our samples. To maximize the impact of this process, any surface preparation of Nb should be performed as close to the deposition process as possible. This ensures the oxide layer does not build up significantly. Samples in Round 2 were able to undergo BCP and spray within a span of 4 days. As soon as the samples underwent BCP, they were bagged and sealed in nitrogen purged bags and only opened before spraying.

Before a sample is sprayed, a sample is used for calibration of spray parameters. This essentially passes if two parameters are met, the coating adheres to the substrate and the spray thickness is consistent with the calculated thickness. Due to a lack of adhesion during Round 2 calibration spraying, the pre-spray preparations shifted. The experimental design of the remainder of Round 2 was changed at this point to prioritize adhesion. Samples underwent either grit blasting, bond-coating, or a combination of both. Bond coating was done with a metal matrix composite called Nano Al-Trans, a powder by Inovati. This bond

coat is presented in more detail in the following section.

3.3 Powder Preparation

Different copper powder was used for Round 1 and Round 2. These powders were procured from Praxair as Cu-159 powder. The powders used during Round 2 testing were provided by North Carolina State University (NCSU) and this powder was sieved in an inert gas glove box to minimize oxygen pickup. All powder used is spherical, an SEM image of the powder is shown below taken by Dr. Tim Horn's lab at NCSU.

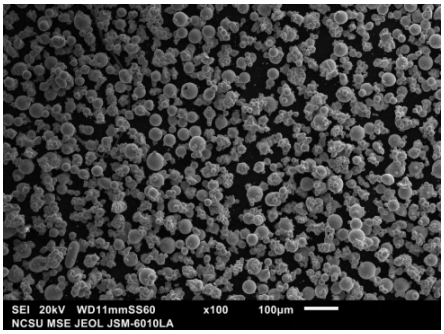

Figure 37: SEM Image of Praxair Cu Powder for Round 1 by NCSU

Powder analysis was performed on both powders from Round 1 and Round 2 via a Microtrac analysis. Microtrac particle size distribution (PSD) is given for the powder heat used in Round 1 and Round 2. Round 1 achieved a PSD of 17 microns for d90 and Round 2 achieved 22 microns for d90. To explain, a distribution of 17 microns for d90 represents 90% of powder consisting of 17 microns and below. This is not the best representation of powder, so including measurements of d10 and d50 help to understand the PSD more.

Table 2: Particle size distribution of powder from Round 1 and Round 2

Microtrac PSD	Round 1 Praxair - 2015	Round 2 Praxair - 2018
d10	8µm	5µm
d50	11µm	13µm
d90	17µm	22µm

In order to spray the Cu powder, a hopper is loaded with the powder before connecting to the spray chamber. Any powder that is sprayed is placed into a vacuum furnace to bake out any moisture at 'low' temperatures of 50-100C. Reducing moisture ensures the powder to flow freely during deposition feed and

doing this in a vacuum environment ensures minimal oxygen pickup at elevated temperatures. To minimize oxygen pickup, the powder was sealed and placed in a dehumidified vacuum chamber until needed. To load the powder into the chamber, a large barrel was used and the hopper was placed at the bottom. Argon gas was loaded into the barrel and due to the density it is assumed the barrel is full of Argon gas and minimal oxygen. The Cu powder was opened and poured into this hopper while being held below the top line of the barrel.

(a) Powder loading (b) Feed Rate Scale (c) Powder Heat

Figure 38: Loading powder into hopper while minimizing oxygen exposure. Feed rate of the powder hopper tested for consistency via scale. Powder heat for Round 2 spraying - 23μm

The powder hopper has a sieve that is chosen for the material of choice as well as a metal brush that pushes the powder through the sieve for consistent deposition. To ensure the powder has a consistent feed rate, the hopper is placed into a weigh pan and set to deposit at a constant rate for 30 seconds. The resulting powder is weighed, and the process is repeated for a minimum of 3 tests. If the deposited powder weight remains consistent then the feed rate is consistent and will perform as expected during the spray process. The powder morphology, size distribution, chosen feed rate, and whether or not the powder has any moisture are all factors on getting the powder feed rate to be constant. This process of calibrating feed rate is also carried out for grit blasting.

The powder that was used as a bond coat during Round 2 is Inovati's Nano Al-Trans, consisting of a two phase nano aluminum powder with SiC grit dispersed. This powder is used because it can create a very thin coating while significantly increasing metallurgical bonding and adhesion strength. The powder has adhesion strength corresponding to ASTM C633 at 10ksi with epoxy failure, adhesion to substrate passes ASTM B571, near net-zero porosity, high conductivity, and is fully dense [16].

3.4 Cold Spray Parameters

Parameters of cold spray were a summation of our desired outcome, our brief knowledge of CS, and Inovati's expertise. The spray parameters that are to be controlled by Inovati are feedrate, travel speed, standoff distance, gas temperature, and gas pressure. The travel speed and feed rate are primarily used to optimize the powder flow and provide a desired deposited layer thickness. The standoff distance is more or less standard for most spray materials at Inovati. The gas temperature and gas pressure are the parameters that cause a strong impact on deposition characteristics. An image of samples of Round 2 being sprayed is shown below. Something to note is that the samples are mounted to the base plate via thick double-sided tape, this works well enough for these samples but this could be a concern for heat buildup in future experiments. Mounting CS samples is difficult as any area between CS samples is also sprayed. Because of this, small samples such as these cannot easily be mounted onto a custom plate that provides better thermal conduction away from the substrate surface as sample removal would prove difficult if Cu coating connected the mount and samples. Thus the tape was the chosen method and recommended as sufficient by Inovati.

Figure 39: Cu coating of 13 samples in Round 2

Once the powder was loaded into the hopper, the deposition parameters that were decided are shown in the table below. Something not listed in the spray parameters is the spot size of the powder impacting the substrate. The spot size of the metal powder, both the bond coat and Cu coating, is approximately 1/8"in or 3mm while the spot size of the grit blasting is larger and unknown.

Table 3: Deposition parameters of grit blast, bond coat, and each spray

Deposition Parameters

Deposition Info	B4C (100 Grit)	SiC (100 Grit)	Nano-Altrans	Round 1	Round 2
Gas	He	He	He	He	He
Pressure (psi)	90	90	60	70	70
Gas Temp	None	None	400 F	600 F	600 F
Standoff	1 cm	1 cm	1 cm	1 cm	1 cm
Feed Rate (g/min)	50	50	12	28	25
Feed Rate (g/sec)	0.83	0.83	0.20	0.47	0.42
Siv used	-	-	35	250	250
Spray Arm Speed (in/sec)	-	-	24	5	4.5
Spray Arm Speed (mm/sec)	-	-	609.6	127	114.3
Thickness	-	-	0.031 mm	0.55 mm	0.6 mm
Step Size	-	-	0.01"	0.02"	0.02"
Estimated Velocity	-	-		700 m/s	700 m/s

The parameters chosen for both abrasive medias used are standardized by Inovati. The spray parameters for Nano Al-Trans bond coat are also standardized by Inoavti and the main takeaway here is the designed spray thickness of 0.031 mm (31 microns) chosen to minimize the impact of the bond-coat on the sample while maximizing the adhesion strength throughout the Nb/Nano Al-Trans/Cu interface. The parameters chosen for Cu CS from Round 1 and Round 2 utilized the same gas and pressure of Helium at 70 psi. Reminder that KM utilizes a unique nozzle that enables HPCS velocities at reduced pressures, so this pressure is not conducive with most CS pressures. The main difference between spray parameters of Cu from Round 1 and Round 2 are the coating thicknesses. These are different mainly because with a new powder, a new calibration is needed to be done and the thickness of a single layer was aimed to be close between 0.5 - 0.6 mm which was achieved for both rounds. The estimated velocity is provided by Inovati via a proprietary equation. This velocity is estimated and assumed to vary slightly due to the difference in PSD of the powder.

3.5 Heat Treatment

Samples were separated into two sections, heat treated (HT) and non-heat treated. For every sample parameter chosen, there is at least one sample that has been HT and one that has not. The Across International STF-1200 Tube Furnace has a 300mm long hot zone with a 72mm quartz tube inner bore, capable of controlled furnace cycles up to 1100°C. The system is pumped using a combination rotary vane/diffusion pump. The vacuum was able to achieve 0.01 mTorr.

The furnace was calibrated for correct parameters, it was found that the internal temperature differed from the externally measured furnace temperature by an offset of 20°C. To ensure proper furnace cycles,

calibration of this temperature control was performed with CuSil braze alloy with a firm melting temperature of 780°C. An internally routed thermocouple read directly to a NIDAQ controller was then correlated with the furnace PID control values in MATLAB. Multiple trials were run so that the offset was understood properly. Additionally, trials were run to determine the steady state time required to reach each of the desired temperatures of 250°C, 600°C, and 800°C as the internal temperature lagged behind the external PID control. Using the optimized steady state time and temperature offset, a furnace cycle was created for heat treatment of the CS samples. Below, the furnace is shown on the left and the MATLAB calibration plots are shown on the right.

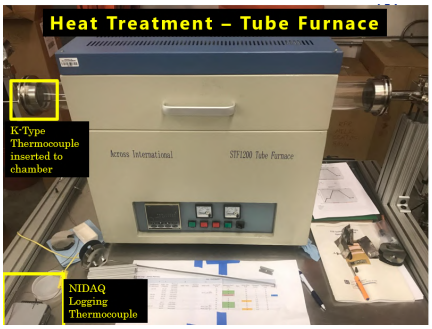

(a) Tube Furnace

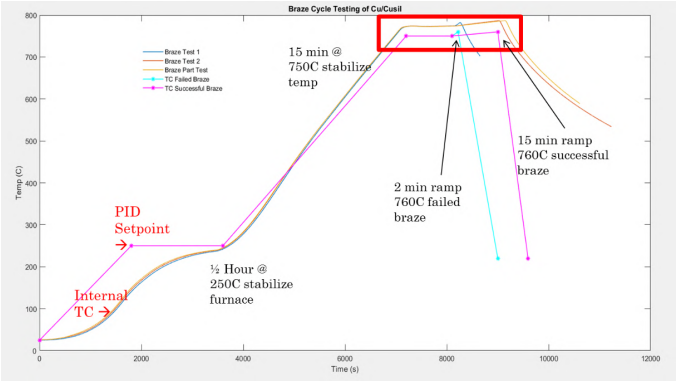

(b) Furnace Test

Figure 40: Furnace development with (a) vacuum tube furnace used in study and (b) furnace tests in MATLAB from an internal TC connected to a NIDAQ controller to find temperature offset

Using the CuSil eutectic melting temperature of 780°C as our reference, we determined from these trials that the internal furnace temperature is +30°C +/- 5°C higher than the internal programming temperature, likely due to poor PID tuning and/or a malfunctioning thermocouple. CuSil wetting of Cu was imaged in an SEM to verify proper braze conditions.

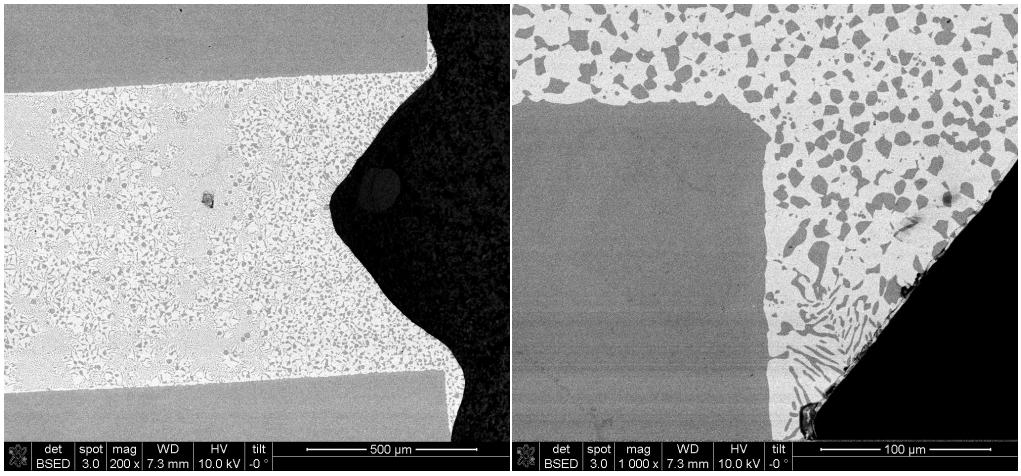

Figure 41: SEM image of Cu and CuSil after a successful braze

Nevertheless, it was decided that we could tolerate these uncertainties in the annealing schedule, and decided to run our PID program at 770°C, which we concluded corresponds a sample temperature of 800°C.

The annealing cycle for the CS samples has 3 parts. The first stage is ramping to 250°C which is the recommended holding temperature for the furnace before ramping to anything else. The second stage is 600°C for 1 hour for the purpose of hydrogen degassing of Nb. While the furnace is not connected to an RGA as originally hoped, the pressure sensor is noted to increase to 0.05 mTorr during this stage before decreasing down to 0.01 mTorr at the end of the second stage. This correlates to the study done at Argonne National Lab for a half-wave resonator cryomodule in which hydrogen degassing occurred significantly at 625°C and the pressure increased to 5E-5 Torr before returning to 1E-7 Torr after some time. While it is not known that this hydrogen degassing step affects the CS of Cu onto Nb, hydrogen embrittlement can cause adverse effects that have been discussed in Section 3.2.2. Because of these factors, this additional stage of heat treatment has been adopted as common practice in this study. The third stage is annealing at 800°C for 2.5 hours to anneal the Cu and Nb to relieve thermal and mechanical stresses of both the substrate and coating to recover material properties.

As the vacuum tube furnace was not leak checked, additional precautions were taken to avoid unwanted oxidation of the Cu/Nb samples. This was done by surrounding the samples in a CP-Ti shimstock that has been tack welded to encase the sample. This proved beneficial as the Ti showed signs of slight oxidation after heat treatment and the two samples that were heat treated without this technique seemed to have a slightly less dull orange color. These indications are all qualitative and there was no method done to verify the leak rate or presence of gases, so the Ti shim was used as a precautionary method as the setup was not difficult or costly.

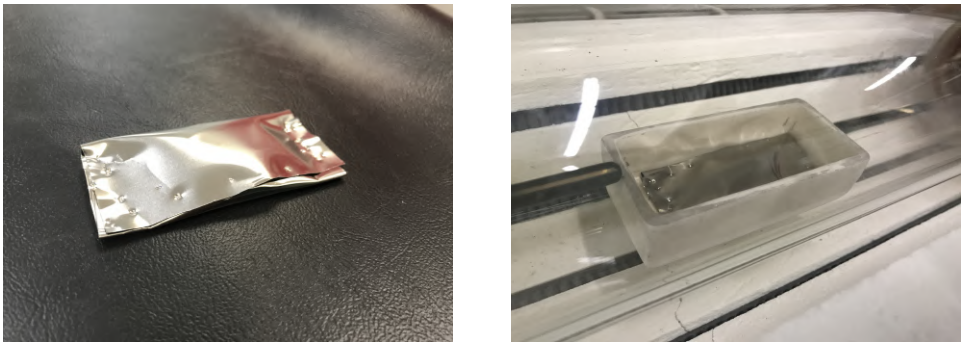

Figure 42: CP-Ti shimstock used to encase samples to grab possible oxidation contamination during heat treatment

3.6 Characterization

Characterization includes analytical techniques such as mechanical testing and microscopy. RadiaBeam has established a metallographic sample preparation lab, including a low-speed diamond saw, abrasive saw, vacuum epoxy mounting and grinding and polishing capabilities. Chemical etching facilities are also available for analysis of grain structure.

3.6.1 Eddy Current

As good thermal conductivity is a requirement for success of this application of cold spray, eddy current was used to correlate electrical properties to thermal properties of the Cu coatings through the Wiedemann-Franz Law. The room temperature (27°C at RadiaBeam) electrical conductivity of the cold spray copper was measured with a SimgmaScope SMP10 eddy current probe, which operates at a 480kHz frequency, corresponding to a maximum skin depth of 0.09mm, much thinner than the copper coating. A brief experiment was performed to prove that the surface roughness of the Cu coating had no effect on the eddy current measurements.


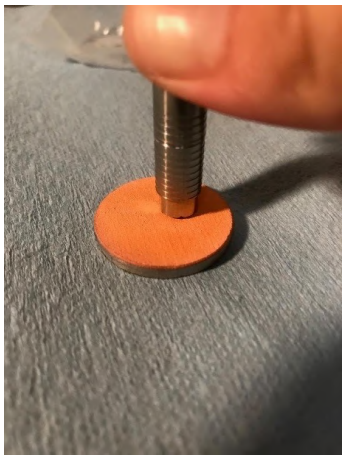

Figure 43: Eddy Current setup and sample measurement

Eddy current was taken for each sample and was recorded pre and post heat treatment for samples that fall under this category. Measurements were always taken in sets of 5 to allow for more accuracy. The eddy current value is displayed in % IACS which is the percent of conductivity in relation to pure Cu and stands for Internationally Annealed Copper Standard. This standard is a simplification of electrical conductivity measurements done in SI units of siemens per meter (S/m) and Oxygen-Free Cu will measure 101% IACS [50]. This value can be correlated with thermal conductivity with the use of the Wiedemann-Franz Law [51]. First, the eddy current measured as % IACS needs to be converted to electrical conductivity. To do so, we take a value of 100% IACS that is known to equate to 5.8001 x 10^7S/m. Next, we take the equation of the Lorentz constant

$$L = \frac{k}{\sigma T} \tag{4}$$

to relate electrical and thermal properties. Where L is the Lorentz value in 10^{-8} Watt*ohm/K^2, k is thermal conductivity in Watt/meter*Kelvin, σ is electrical conductivity in S/m, and T is temperature in Kelvin. With a Lorentz value of 2.23 at 273K, a temperature of 300K, and a known % IACS, the formula can be rearranged to find the thermal conductivity as such:

$$k = \frac{\%IACS}{100} \times \sigma \times L \times T \tag{5}$$

The electrical conductivity of copper should roughly reflect on the thermal properties available for the coating. This needs to be understood for the performance of the coating at cryogenic temperatures, the intended application of this spray pair. While the thermal conductivity is different at cryogenic temperatures, understanding the electrical and thermal conductivity of the coating at room temperature

gives insight into how the material will perform under different circumstances. This insight is extremely helpful for this level of study in offering an applicable comparison between samples.

3.6.2 Adhesion Testing

Adhesion testing was performed at Inovati using an Elcometer 510 adhesion tester with a custom mounting block which accommodates our specific sample size, which is shown in Figure 44. The metal plate sits on the flat surface, the lower surface of the sample under test (SUT) is epoxied into the circular cavity, while the upper surface is epoxied onto a puller pin. Shims are placed around the sample to create a level surface for the adhesion tester. Once epoxy has dried, an instrumented grip pulls on the puller, with a counteracting force being applied to the levelled mounting block. For our Cu/Nb coupons, failure can occur in three ways: at the Nb/Cu interface, the epoxied Cu/puller pin interface or at the epoxied Nb/mounting block interface.

(a) Adhesion Tester

(b) Sample post adhesion test

Figure 44: Left: Adhesion tester used in this study and Right: Sample stub after epoxy adheres to cold spray surface

While this adhesion testing method is not as recognized as the ASTM C-633 standard, rapid tests were performed on-site at Inovati, whose experience is that this adhesion tester has very good correlation with ASTM C-633.

3.6.3 Profilometry

Surface roughness measurements were performed in-house at RadiaBeam with a Mitoyo SJ-410 stylus profilometer. The purpose of these measurements is to understand the correlation with surface roughness and the quality of deposition. The value used to relate surfaces is the Ra value. This is essentially the average of all peaks and valleys throughout a particular line scan with the stylus profilometer. For this study, surface roughness for Round 1 samples was all the same with B_4C grit blasted Nb substrates. Round 2 contained 3 different surfaces: SiC grit blast, hand ground with 120 grit SiC paper, and turned samples. For reference, a surface prepared via grit paper has an assumed Ra value if not measured and is

presented in the chart below.

Table 4: Surface Ra values depending on size of abrasive grit

Grit Finish and Estimated RMS and Ra Values

Grit Finish	RMS (Micro-inch)	RMS (Micron)	Ra (Micro-inch)	Ra (Micron)
36	160	4.06	142	3.61
60	98	2.49	87	2.21
80	80	2.03	71	1.8
120	58	1.47	52	1.32
150	47	1.2	42	1.06
USDA Bead Blast	47	1.2	42	1.06
180	34	0.86	30	0.76
220	21	0.53	19	0.48
240	17	0.43	15	0.38
320	14	0.36	12	0.3
400	10	0.25	9	0.23
Mirror	5	0.13	4	0.1

(a) [MicroGroup]

3.6.4 Microhardness

Microhardness measurements were carried out using LECO AMH55 microhardness tester (LECO Corp., USA) with a Vickers pyramidal diamond tip. The measurements were taken at loads 1 kgf across the surface and cross section. Only one sample underwent microhardness measurements due to time constraints, this sample was a sample from Round 2 that consisted of SiC grit blasting, Cu deposition, and heat treatment.

3.6.5 Microscopy

RadiaBeam houses a state-of-the-art Keyence VHX-6000 digital light optical microscope (LOM) for imaging up to 200x. For higher resolution imaging, we have access to a Nova NanoSEM 230 field emission scanning electron microscope (SEM), located in the UCLA Materials Science and Engineering department. This SEM is located in the Electron Microscopy Lab directed by Prof. Sergey Prikhodko of the Materials Science and Engineering department at UCLA. SEM imaging was used extensively and will be presented frequently through the study.

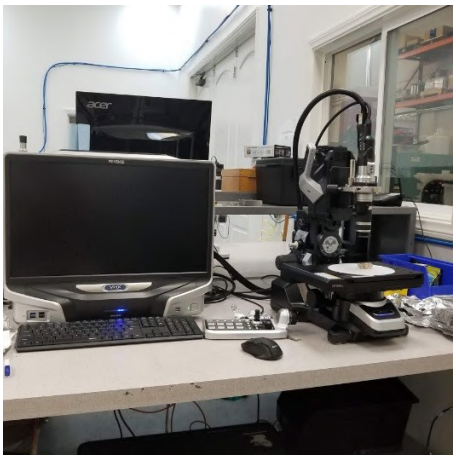

(a) RadiaBeam LOM

(b) UCLA SEM

Figure 45: LOM and SEM used during study with Left: Keyence Microscope and Right: Nova Nano Scanning Electron Microscope

Samples prepared for imaging were mounted in 1.25" epoxy mount and cut with an abrasive saw. These samples were ground from 320-800 grit SiC paper then polished at 1200 grit SiC paper, 9, 3, and 1 micron polycrsytalline diamond, and finally 0.05 colloidal silica polishing slurry. This was performed on an Allied High Tech MultiPrep System. After polishing, the samples are rinsed with water and sonicated isopropyl alcohol to remove polishing media. The polished samples are etched in a solution of Hydrochloric (HCl) and Ferric Chloride ($FeCl_3$) for 20 seconds to reveal Cu grain boundaries [52]. This etchant has no effect on Nb. For etching of Nb samples, the etchant used for BCP discussed in Section 4.2 was used. The samples are then prepared for LOM and SEM imaging.

4 Results and Discussion

The experiments were done in two separate batches, Round 1 and Round 2. Round 2 samples were sprayed with knowledge gained from Round 1 results. The differences between the two batches are presented and discussed. All samples underwent the same analysis and characterization. An SEM image in Figure 46 shows what is to be expected in cross sections of Nb substrate and Cu coating. The table below this summarizes the number of samples that were dedicated to specific process parameters. Round 1 samples were grit blasted with boron carbide and subject to heat treatment, adhesion testing, and cross sectioning.

Round 2 samples were grit blasted with silicon carbide and some samples had a bondcoat applied. These samples were subject to heat treatment, adhesion testing, and cross sectioning in order to understand the effects of each process parameter.

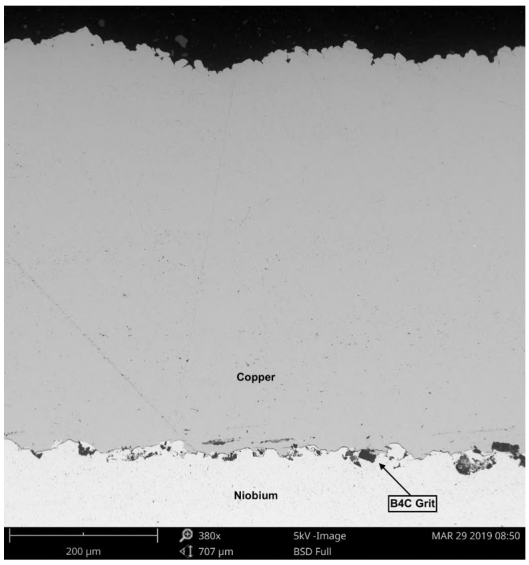

Figure 46: Micrograph depicts what most sample cross sections will look like: Nb substrate and Cu coating

Table 5: List of Round 1 and Round 2 samples with brief summary of post processing

Round 1 List	
6x B4C grit @ 0.5 mm coating	2x 800C treatment / 1x Adhesion Test / 2x Cross Section
5x B4C grit @ 1 mm coating	1x 800C treatment / 0x Adhesion Test / 0x Cross Section
Round 2 List	
4x SiC grit	2x 800C treatment: 1x Adhesion Test / 1x Cross Section
4x Nano Al-Trans	2x 800C treatment: 1x Adhesion Test / 1x Cross Section
4x SiC grit + Nano Al-Trans	2x 800C treatment: 1x Adhesion Test / 1x Cross Section

4.1 Round 1 and Round 2 Process Differences

From the results of Round 1, the goals of Round 2 were primarily to ensure sufficient adhesion. The initial goal of Round 2 was to ensure adhesion without the use of grit blasting. During Round 2 spray, a turned niobium sample was used as the calibration test piece. The calibration test piece serves as a reference to determine if spray parameters result in desired adhesion. The calibration also tests the cold spray setup parameters for coating thickness and travel speed and feed rate. This sample did not adhere and the Cu coating peeled back immediately during deposition. In an attempt to ensure adhesion, the travel speed was increased to create a thin coating. This coating also failed deposition and began to peel after half of the sample was covered. The experimental design of the remainder of Round 2 was changed at this point to prioritize adhesion. It was apparent the surface roughness was not high enough to enable significant

mechanical interlocking. This experimental design change needed to be made during an on-site visit at Inovati and thus silicon carbide grit blasting and application of a bond coat were chosen.

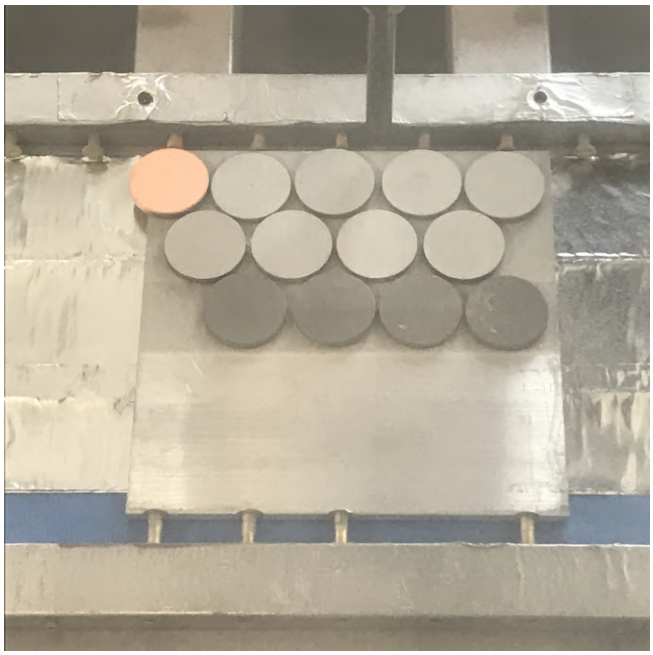

Figure 47: Round 2 samples before Cu deposition consisting of 8x Nano Al-Trans bond coating, 4x SiC grit blast, and 1x Round 1 sample annealed

Samples in the image above are all of the samples from Round 2 after surface preparation and before copper deposition. These consist of: 8 samples that have been coated with a thin bondcoating of Nano Al-Trans, 4 samples that have been grit blast with SiC abrasive media, and 1 sample from Round 1 that has been annealed and will receive an additional copper coating.

4.2 Surface Treatment

A main difference between Round 1 and Round 2 processes is seen in the surface treatment for the purpose of promoting adhesion. It was found that while embedding of grit blasting media was unavoidable, media with higher friability allows for increased adhesion of the coating. Spray parameters of Round 1 and Round 2 remained the same with the main goal of Round 2 being coating adhesion through changes in powder and substrate preparation. The initial goal was to eliminate the use of grit blasting in Round 2 as embedded grit will enhance the effective thermal contact resistance between the Nb and Cu. The gas pressure, temperature, and estimated particle velocity carried over to all samples, as listed in section 4.4. The only differences were in the substrate and the powder. The substrate underwent different preparation techniques from being turned, ground, BCP etched, and grit blasted. These processes were in efforts to enhance

surface roughness and eliminate oxides and contaminates. Grit blasting from Round 1 was performed with B_4C with micrographs of this seen in Figure 48 depicting severe embedding of the abrasive media.

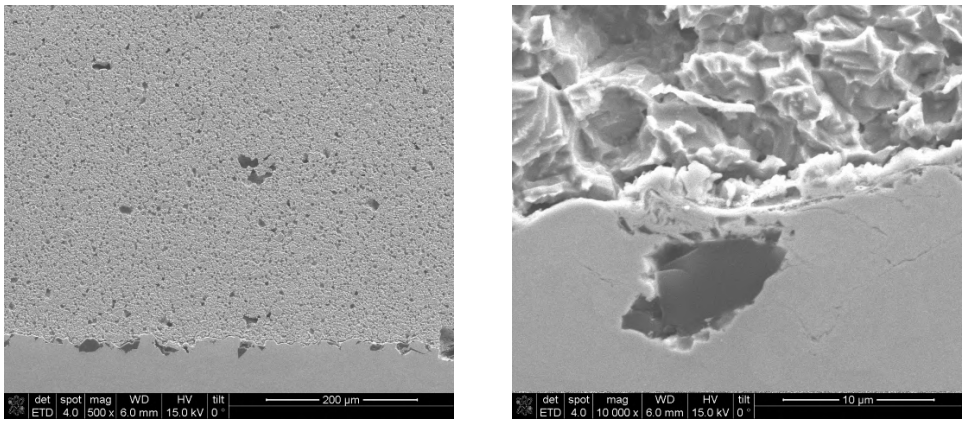

Figure 48: Cross section of B_4C grit blasted interface revealing embedded particle in substrate from Round 1

Cross sectioning of Round 1 samples revealed particles embedding. The particles were fully intact without shattering and even in some places embedded deeply enough to be fully surrounded by Nb. B_4C is a very hard abrasive media as one of the hardest materials created. Embedding of B_4C is predicted as a main proponent inhibiting adhesion of Cu coating in Round 1. Embedding from grit blasting inhibits adhesion through cold work increasing hardness of the Nb substrate and minimizing the surface area allowed for Cu/Nb mechanical interlocking. Because of this, it was proposed to create a fabricated surface roughness through turning Nb samples on a lathe and grinding the surface with SiC 120 grit paper. The goal was to create a surface roughness high enough to eliminate the need for grit blasting and subsequently eliminate any issues arising from embedding. The surface roughness from various preparation is summarized in the table below by Ra values.

Table 6: Ra values from different surface preparation techniques

Surface Preparation	Ra-Value (µm)
B4C Abrasive - Round 1	3.5 +/- 0.2
Turned - Round 2	2.4 +/- 0.7
Hand Ground - Round 2	1.1 +/- 0.1
SiC Abrasive - Round 2	3.3 +/- 0.2

Note that the BCP etching of Round 2 was found to not have a noticeable or statistically significant impact on Ra values. The samples of Round 2 were ground using 120 grit SiC paper resulting in a fairly consistent Ra value of 1.1μm, this is consistent with estimated Ra value of 1.3μm from 120 grit paper. The turned samples of Round 2 show a relatively high Ra value of 2.4μm with a high error. It is important to

interpret these results correctly by understanding how surface roughness measurements are calculated. Ra values are not a tell-all in the surface metrology of a substrate, this is depicted in the turned samples. The turned samples create a fabricated surface roughness measured with Ra without showing the full picture. Accurate surface metrology requires a more in-depth look, as Ra value is found as the arithmetic mean of the assessed profile. Because of this, the sprayed powder cannot be guaranteed to behave as if interacting with a substrate of the measured surface roughness. To elaborate, a surface roughness measured by Ra is an arithmetic average of peaks and valleys without taking into account any distance between these peaks and valleys and the frequency through a given length of a profilometer scan. This can lead to a misleading Ra value in the sense of cold spray technology as seen in Figure 49 where the Ra value is independent of frequency. This changes the angle of incidence and ability for mechanical interlocking and explains why the substrate of turned Nb did not yield successful results.

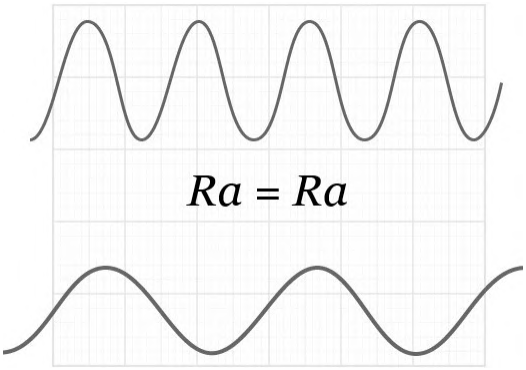

Figure 49: Diagram of signals of different frequencies with the same amplitude resulting in equal Ra values with top: higher frequency and bottom: lower frequency

Understanding these Ra values properly explains the failed calibration sample. The need for other methods to promote adhesion became apparent. The method that was readily available at Inovati was grit blasting and bond coating. Grit blasting of Round 2 samples utilized SiC as it is slightly softer than B_4C.

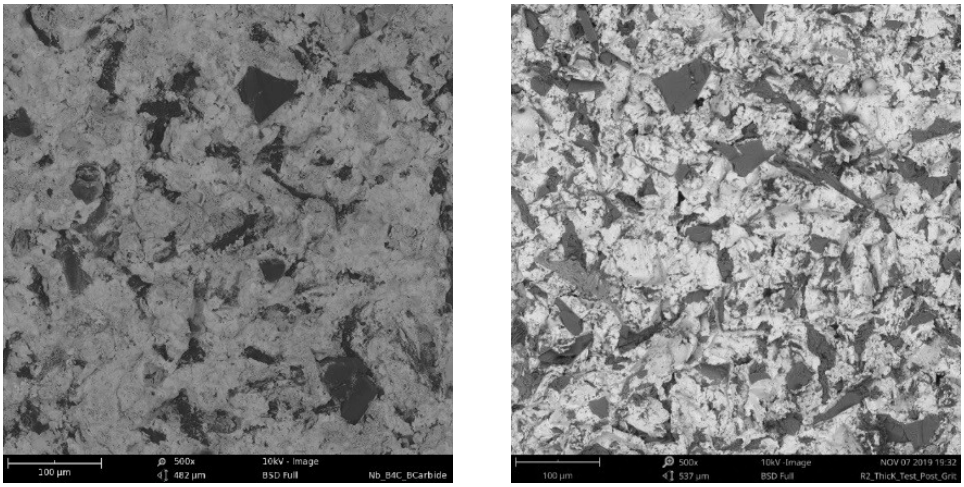

Figure 50: Embedded grit in Nb substrate with Left: B_4C and Right: SiC

This change in media is chosen to reduce impact on Nb substrate and reduce embedding while achieving the same surface roughness as Round 1. Unfortunately, the level of ceramic coverage due to embedding was the same for both media. The main difference seen between both media is shown in the cross section.

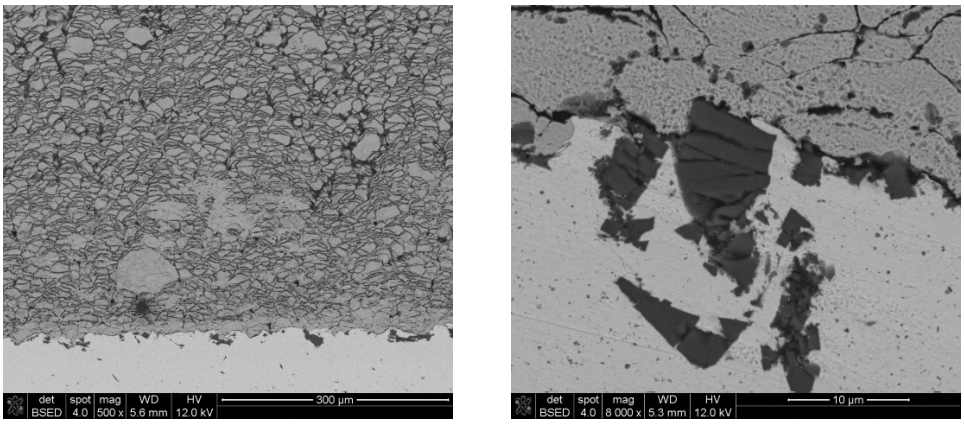

Figure 51: Cross section of SiC grit blasted interface revealing broken SiC particles in Round 2 with Left: view of full interface and Right: magnified view of shattered particle

It is clear that the B_4C media did not shatter while SiC media did. This correlates to SiC being less hard than B_4C, or rather more friable. The difference of these abrasive medias is seen in the higher friability of silicon carbide compared to boron carbide where friability is the tendency of a solid substance to break into smaller pieces under duress. Ceramic shattering is a result of absorbing enough energy. Knowing this it can be assumed that B_4C did not absorb enough energy to cause shattering while SiC did. While knowing the spray conditions of both media were identical and the only difference is the hardness of the media, it is then assumed that the B_4C embedding resulted in a larger amount of energy deposited into the Nb substrate. This creates a larger amount of plastic deformation resulting in a higher increase of

hardness at the surface. The SiC media was able to absorb enough energy upon impact to shatter resulting in less increase of hardness at the surface. At the same time, shattered media could cause a slight increase of available surface area for Cu/Nb mechanical interlocking but this is difficult to measure and thus not a main driving factor. This difference between abrasive media used is a driving factor for increased adhesion from Round 1 to Round 2.

4.3 Heat Treatment

Heat treatment was a key process parameter in comparing samples. The process of vacuum annealing directly impacted electrical conductivity and adhesion and resulted in findings related to degassing, stress relief, and microhardness. As a reminder, vacuum annealing of samples was done at 600°C for 1 hour and 800°C for 2.5 hours.

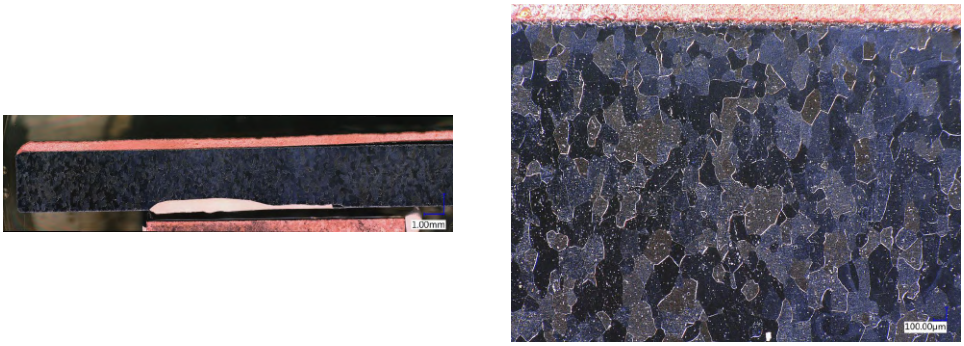

Figure 52: LOM cross section of cold spray interface after thermal annealing and etching

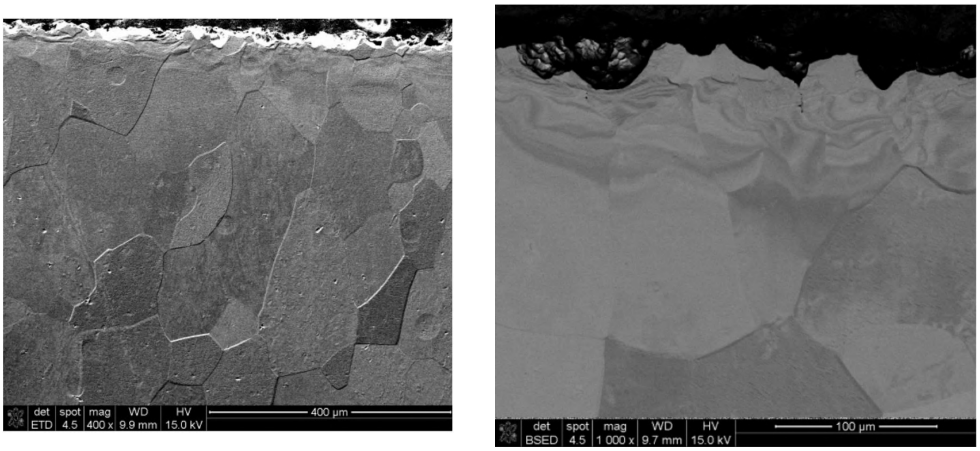

Figure 53: SEM cross section of cold spray interface after thermal annealing with Left: lower magnification of Nb grains and Right: higher magnification of Nb plastic deformation

This etched cross section of Nb at the interface post heat treatment reveals an area of plastic deformation seen near the Nb surface of Figure 53. This sample underwent grit blasting of SiC abrasive media in Round

2. As grit blasting has been proven to cause an increase of hardness, this plastic deformation reveals that there is most likely an increase of hardness at the substrate surface which, based on literature, would inhibit adhesion. There is no etched Nb interface of Round 1 samples that were blasted with B_4C abrasive media, so it can only be assumed that this harder abrasive media possibly caused a larger area of plastic deformation than SiC. This etch also reveals that our heat treatment is not enough to cause full recrystallization of Nb as there is still plastic deformation. There is stress relief in the Nb bulk as seen in proceeding microhardness tests. Stress relief must also occur in Cu coating but is difficult to show without full microhardness tests.

Heat treatment results in many important changes. These changes are highlighted when looking at microhardness, coating thickness, conductivity measurements, and various micrographs. One resulting change from heat treatment is microhardness. However, not enough samples or indentations were made to merit microhardness a section of it's own and are presented immediately. Microhardness testing reveals that the bulk Nb rod from which all Nb substrates originate appears to be cold worked and is highlighted on the outer edges of the rod. This is seen by an increase from 62 HV to 70 HV between the center and edge of wrought Nb sample. The edge is denoted as anything 1 mm or less from the edge. While the edges highlight a large amount of cold work through processing, it is not unlikely that the entire Nb sample has stored energy from processing. After heat treatment this hardness decreases significantly to 51 HV and 67 HV center and edge respectively.

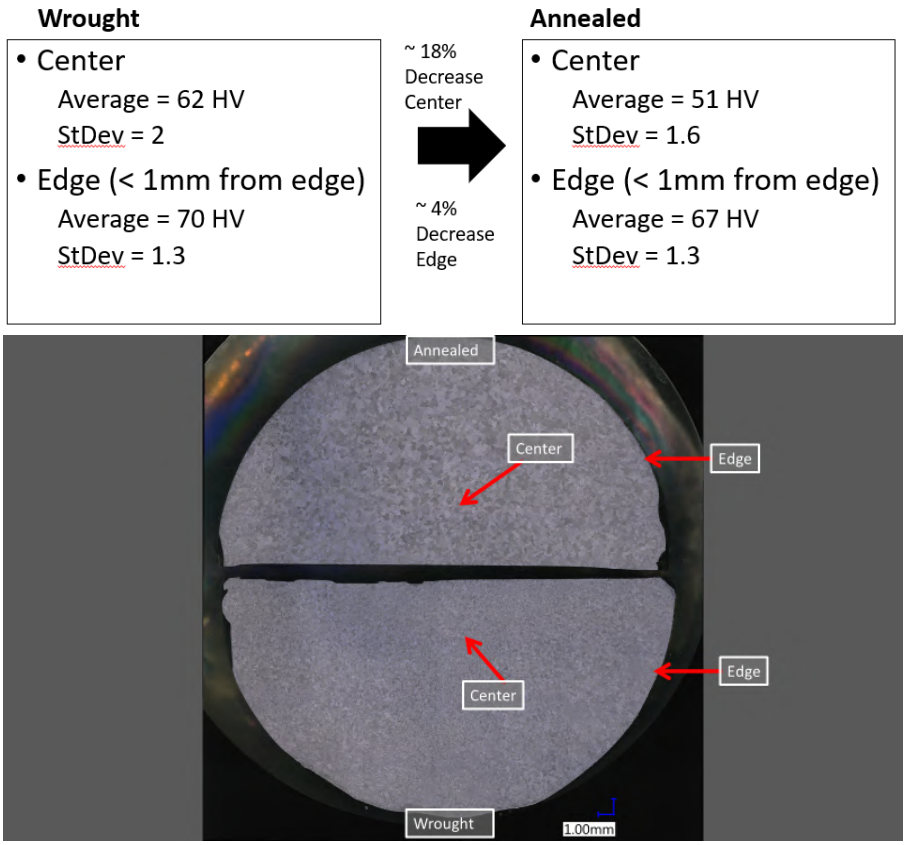

Figure 54: Microhardness of Wrought vs Annealed Nb with a summary of differences

While the hardness of the Nb substrate after heat treatment is helpful, the more important measurements are of the Nb at the interface and any Cu coating. In this study, only one interface was measured for microhardness.

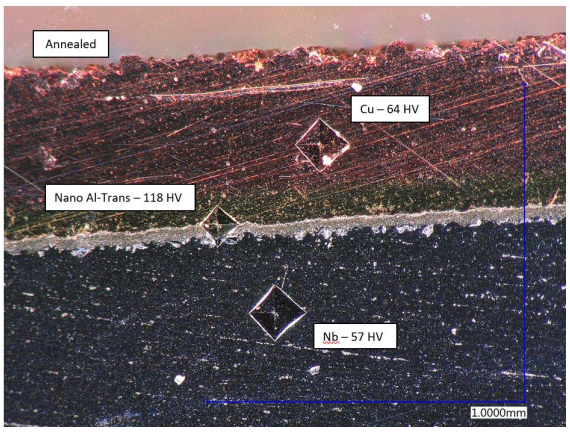

Figure 55: LOM cross section of bond coat cold spray sample post-annealing with microhardness indentations of each layer

The lone sample measured was from Round 2 and consisted of Nb/SiC grit blast/Nano Al-Trans/Cu after

heat treatment. This shows a hard bond coat at 118 HV with a relatively soft Cu coating at 64 HV. The substrate of Nb shows 57 HV after annealing. The values that would be of interest are the Nb substrate at the interface before deposition, after grit blasting, after deposition, all pre and post heat treatment. The purpose would be to expand upon the finding of a plastic deformation zone in the Nb substrate.

4.4 Conductivity

As electrical conductivity is important to understand the potential of a Cu coating, the eddy current was measured pre and post heat treatment. The eddy current can be converted to a thermal conductivity estimation to offer insight into the properties at varying temperatures. As RRR measurements were not conducted to understand the coating properties at cryogenic temperatures, these measurements are the only insight into electrical and thermal properties of the coatings in this study. The eddy current in the measurement of %IACS is shown below.

Table 7: Eddy current measurements of all samples throughout the trials with thermal conductivity estimation compared to OFE Cu

Round 1					
Sample Description	Eddy Current Pre-Annealing (%IACS)	Eddy Current Post-Annealing (%IACS)	Δ%IACS	% Recovery	Final Thermal Estimate (W/mK)
B4C grit + 0.5 mm	55	86	31	56	335
B4C grit + 1.0 mm	57	88	31	54	344
Round 2					
SiC grit	50	89	39	78	346
Nano Al-Trans	49	89	40	82	346
SiC grit + Nano Al-Trans	50	89	39	78	346
OFE Cu	101	-	-	-	391

It is found that the conductivity is able to recover largely through annealing. The electrical conductivity of Round 1 as sprayed samples averaged 56%IACS with no significant difference between 0.5mm and 1mm coatings. Round 1 was able to recover with an increase of 55% to 87%IACS. The electrical conductivity of Round 2 as sprayed samples averaged 50%IACS across all samples and was able to recover with an increase of 80% to 89%IACS. This suggests that the bulk Cu portion of the Round 1 coating was of higher quality than the as-sprayed Round 2 coating. However, Round 2 appears to be the higher quality coating as the final conductivity is higher. It was originally assumed that the properties of the as-sprayed coating would be directly proportional to any change of properties after annealing. There seems to be more factors than can be found through eddy current measurement alone. In this case, factors impacting the coating quality are the substrate preparation, the oxidation of the Cu powder, and the powder morphology/PSD. The spray parameters remained the same between Round 1 and Round 2 with only a small change in coating thickness. To summarize, Round 2 coatings carry more desirable properties after

annealing while Round 1 samples carry more desirable properties before annealing. SEM micrographs offer insight into the differences between these coatings and why they were both able to recover so extensively.

Note the eddy current measurement depth does not measure all the way through the surface coating of any thickness in this study. The measurement depth of the device used ensures that only the Cu coating is involved in the measurement. While eddy current does not necessarily take into account the entire bulk sample such that a RRR test would accomplish, the measurements have been tested to be consistent regardless of surface roughness and are sufficient for the scope of this study.

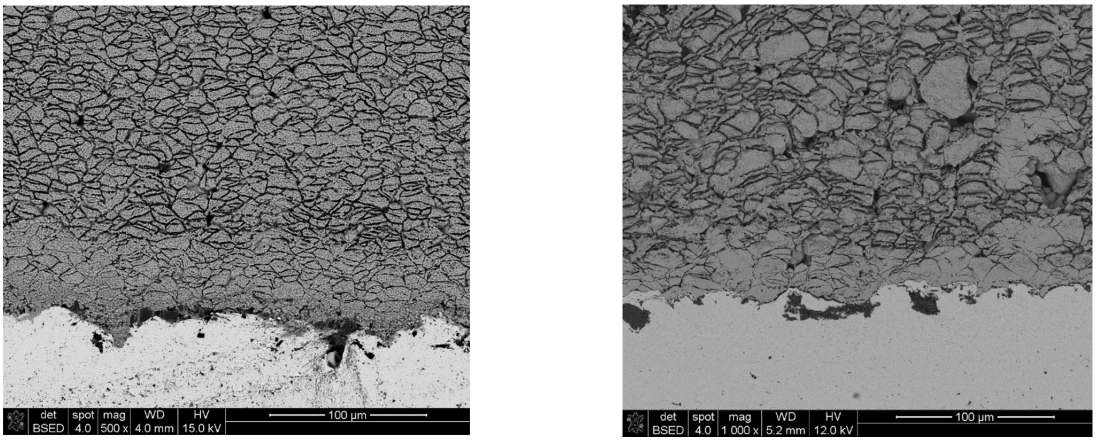

Figure 56: SEM micrograph depicting tamping effect seen in Round 1 (Left) and Round 2 (Right)

The tamping effect is the cause of subsequent powder deposition causing compaction and densification of previously sprayed layers. The tamping effect can be seen in both Round 1 and Round 2 at the Nb/Cu interface. The samples shown in the images above have not gone through annealing. The tamping effect is not seen in annealed samples, the assumption is that annealing allows for stress relief of the cold-worked particles and thus would not be seen as clearly as before annealing. Round 1 appears to have a higher tamping effect with approximately 50μm of significantly compacted powder while this compacted zone in Round 2 is reduced to 25μm. However, on the scale of a coating of 500μm, a difference in tamping effect of 25μm is not enough to explain a difference in the coating qualities. The tamping effect is heavily seen at the interface with significant compaction, but recalling Stage 3 of CS the bulk coating can be densified without the severe deformation seen in Figure 56. This densification can create a decrease in porosity throughout the entire coating that is not as clearly seen as the tamping effect at the interface. This bulk reduction in porosity can effect the properties of the coating but it is unclear if this can be seen through the small skin depth of our eddy current measurement as the porosity reduction is more prevalent the closer to the substrate interface.

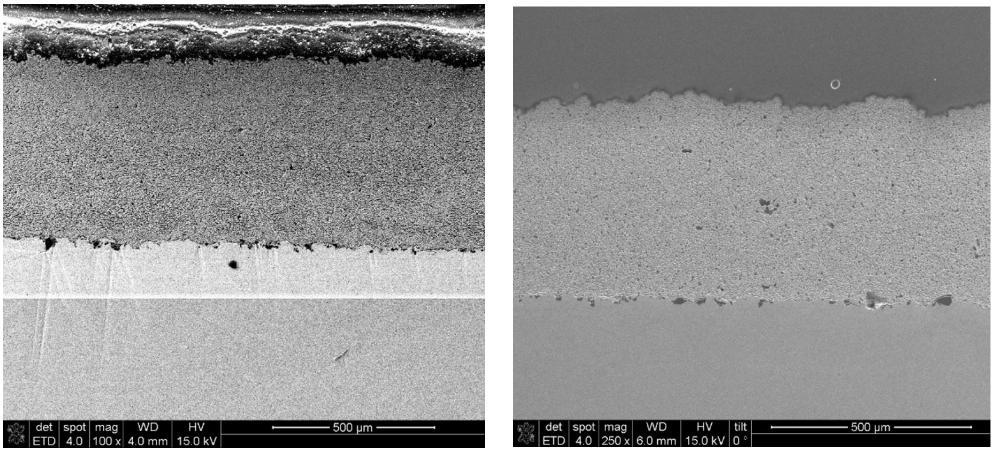

Figure 57: Full view SEM micrograph of Round 1 before annealing (Left) and Round 1 post annealing (Right)

A full view of the coated Nb/Cu interface from Round 1 before and after annealing are shown above. Porosity can be difficult to see when samples have been etched. A few extra seconds of etching after polishing can eliminate the clarity of a cross section. From these cross sections, the significant amount of porosity found in Round 1 does not appear to decrease after annealing.

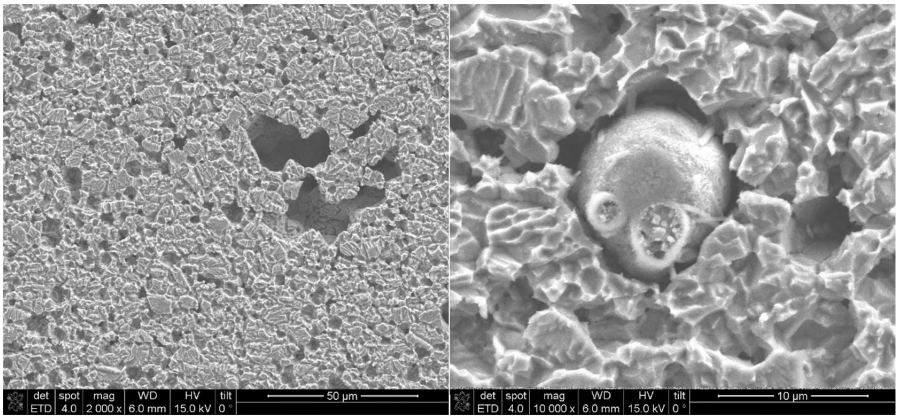

Figure 58: SEM images of Round 1 sample post heat-treatment depicting large porosity (Left) and fully intact particles (Right)

The porosity of Round 1 samples after annealing is prevalent in Figure 58 with large voids seen throughout and particles that were not subject to any deformation. After looking closer, SEM images reveal a number of large pores scattered throughout the coating amongst even more smaller pores. It was alarming to find fully intact particles in the coating without any amount of deformation. This amount of porosity and poor densification can explain the lack of electrical conductivity recovery compared to Round 2.

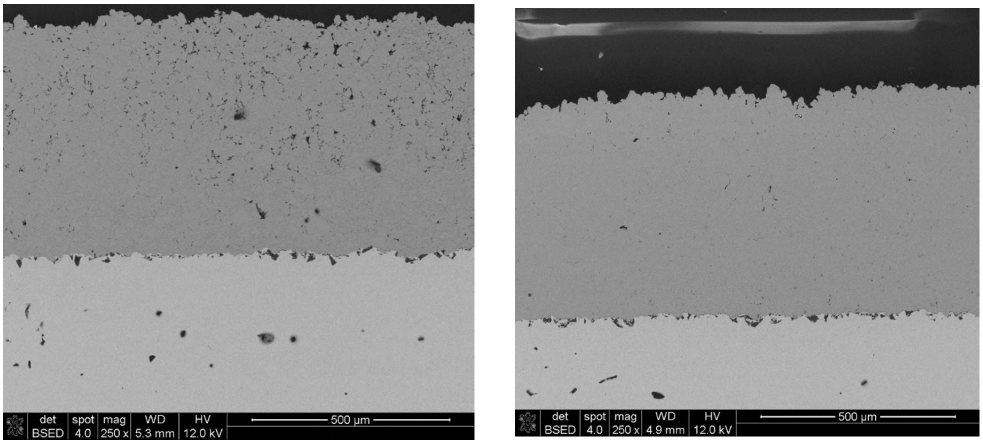

Figure 59: Full view SEM of Round 2 before annealing (Left) and Round 2 post annealing (Right)

After annealing of Round 2 samples, porosity is seen to reduce. Porosity is seen in the coating of Figure 59 before annealing and increases the further from the Nb interface. The porosity is seen in the dark contrast voids in the Cu coating that increase in number and size further away from the Nb substrate. This same porosity is seen to decrease after annealing.

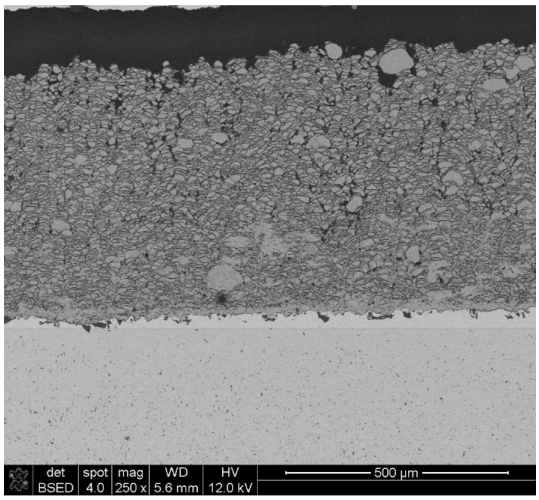

Figure 60: SEM micrograph of Round 2 sample before heat-treatment depicting large particle sizes and porosity throughout the coating

Round 2 micrographs before annealing reveal some particles larger than the sieved 25μm. The particles reach 50μm and result in a PSD of Round 2 powder that is different than originally expected. The number of these larger particles does not appear to be overpowering enough to change the critical velocity of the powder deposition, but this is a possibility.

4.5 Adhesion

Adhesion is the first requirement for a successful coating. A Cu cold spray coating with high conductivity is worth nothing if not bonded to the substrate. Thus testing the quality of adhesion quantitatively helps us understand the impact of design parameters on the adhesion. To begin, thickness measurements were taken with a digital micrometer before spray and between each step of grit blasting, applying a bond coat, and depositing Cu. The table below displays the thickness measurements. Also, the bond coat layer deposited averaged 30μm, a thickness recommended by the expertise of Inovati to be sufficient.

Table 8: Coating thickness of each layer of coating from all samples of both rounds

Layer of Sample	Average Thickness (µm)
Grit Blast	0-10
Nano Al-Trans	31
Cu Coating - Half of Round 1	500
Cu Coating - Half of Round 1	1000
Copper Coating Round 2	600 +/- 5
Niobium Substrate	3 mm

The most relevant relationship discovered in the table above is between the thickness of Cu deposition and the adhesion strength of that coating. Coatings in the case of Round 1 have a higher bond strength with less thickness. This could be due to a decreased thermal/mechanical stress build up during deposition or other factors. The thinner coatings also do not delaminate during heat treatment which could be a result of the stress build up or the lesser impact of CTE mismatch. This can be seen from Round 1 samples where 0.5mm adhered during heat treatment while 1mm delaminated through handling.

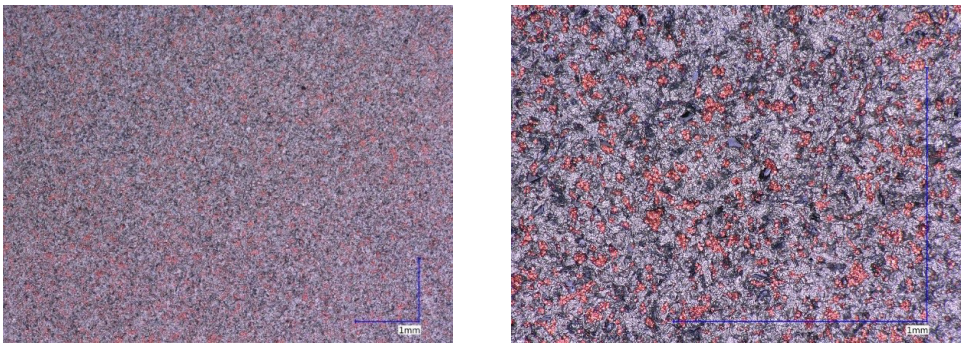

Figure 61: Top down view of Nb substrate after thermal delamination at low and high magnification of Keyence LOM

A sample from Round 1 underwent thermal delamination during heat treatment revealing the B_4C embedded in the Nb substrate. It is seen that a small amount of Cu powder remains adhered to the surface leaving a large amount of the Nb surface and embedded media unaffected by the Cu coating. The cause for

delamination is most likely a combination between the Cu/Nb CTE mismatch and the lack of initial adhesion from deposition. This suggests what was already assumed, that the adhesion strength must be greater than any CTE mismatch that occurs through heat treatment and cryogenic temperatures.

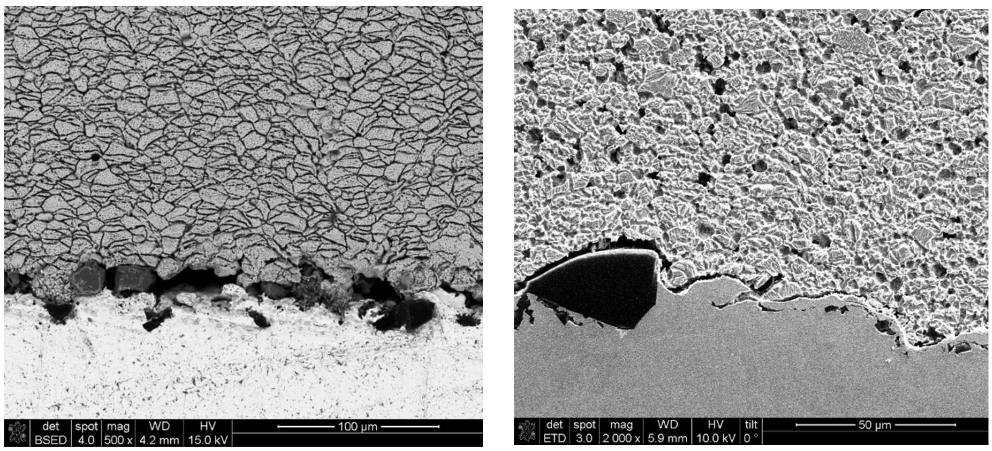

Figure 62: SEM of Round 1 before annealing (Left) and post annealing (Right) showing lack of mechanical interlocking

Looking directly at the interface of Round 1 samples correlates with adhesion results and delamination. The Cu coating does not appear to have a noticeable amount of mechanical interlocking as desired for the copper and niobium spray pair. Because of the results of Round 1, Round 2 samples were sprayed all with 0.6mm thickness until further development guaranteed adhesion and larger thicknesses could be achieved. It is important to note that with optimal design parameters, increasing final coating thickness from 0.5mm to 1mm should not have such a noticeable negative impact on adhesion. However, this was the case in Round 1 with non-optimal parameters and thus the variable of coating thickness was completely removed as the study continued.

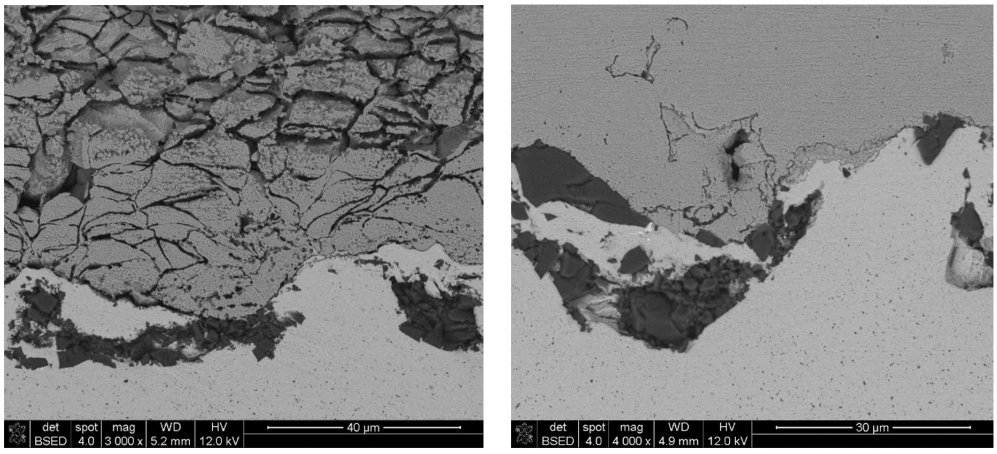

Figure 63: SEM of Round 2 before annealing (Left) and post annealing (Right) showing small amount of mechanical interlocking

Looking directly at the interface of Round 2 samples shows a significant difference from Round 1. While a high level of mechanical interlocking is not shown, the Cu/Nb interface appears much more connected than that of Round 1. This can be attributed to the change of grit blasting media, a slightly larger particle size distribution, and decrease in powder oxygen content from Round 1 to Round 2. The decrease in oxygen content of the powder is discussed in Section 4.6.

For the samples that were able to make it to adhesion testing in Round 1 and all samples in Round 2, the results are presented in the table below. This table does not include samples of 1mm thickness as none of these samples made it to adhesion testing intact, samples labeled Round 1 are to be considered 0.5mm.

Table 9: Adhesion test results in MPa from Round 1 and 2

Sample	Adhesion Strength (MPa)
Round 1 - Annealed	Delaminated
Round 1 - Non-Annealed	18.2
SiC	20.3
SiC Annealed	48.1*
SiC + Bond Coat	31.2
SiC + Bond Coat Annealed	24.9
Bond Coat	46.9
Bond Coat Annealed	37.5*
* = epoxy failure	

Adhesion testing from Round 1 does not reveal much as most samples did not make it to this step. So right away, we see a significant increase in adhesion strength from Round 1 of 18MPa to Round 2 of 48MPa.

The large increase in adhesion strength can be explained through multiple factors of grit blasting, BCP etching, low oxygen, and powder PSD with abrasive media and oxygen content contributing more than other factors. Grit blasting media of SiC allowed for a high surface roughness without the same impact on the substrate as B_4C. This meant that the substrate of Round 2 did not undergo as much plastic deformation and increase of microhardness as Round 1, resulting in increased adhesion strength. The effects of BCP etching cannot be directly seen in these images but is considered a contributing factor despite being unable to quantify the extent of the contribution. Low oxygen content powder has been proven to allow for better adhesion and while not currently quantifiable is considered to be a large contributing factor to the increase in adhesion strength. Powder particle size distribution also contributes to the adhesion strength. As particle size decreases, the critical velocity required for deposition increases. The deposition energy is a summation of the kinetic energy of the powder depending on temperature, velocity, size, and morphology. Round 2 powder has a larger average size distribution than Round 1 and by being sprayed at the same temperature and velocities, this suggests that Round 2 powder contained more

deposition energy than Round 1. This increase in deposition energy (increase in average particle size) from Round 1 to Round 2 is a contributing factor in the increase of adhesion, while it is difficult to say how much of a contribution this difference made.

Bond coating has not been fully discussed yet as these samples do not fully align with the final application of the Cu/Nb spray pair. However, these samples serve as insight into possible bond coat design parameters if explored further. 8 samples had a bond coat consisting of 4 samples with the bond coat applied directly to the Nb substrate and 4 samples with SiC grit blasting before the bond coat was applied. There are no images presented of grit blasted + bond coated samples. The adhesion results show that there is a negative effect from grit blasting before applying a bond coat in this case and there is no apparent need to explore further.

Samples with a bond coat appear to have a decreased adhesion strength post annealing. This is explained by looking at the cross sections of such bond coated samples.

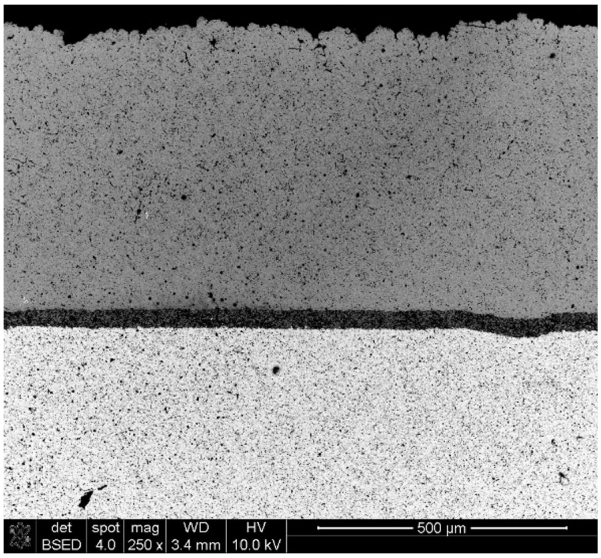

Figure 64: SEM micrograph of Round 2 bond coat before annealing

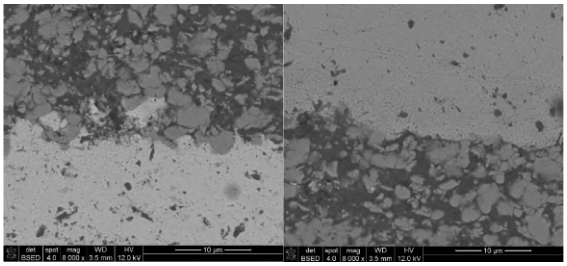

Figure 65: SEM images of Round 2 bond coat before annealing with Nb/Nano Al-Trans interface (Left) and Nano Al-Trans/Cu interface (Right)

The interface between the niobium and bond coat of Nano Al-Trans as well as the interface between the Nano Al-Trans and copper both show good connection with mechanical interlocking and assumed metallurgical bonding. This is from the Nano Al-Trans being a metal matrix composite composed of Aluminum powder and SiC particles.

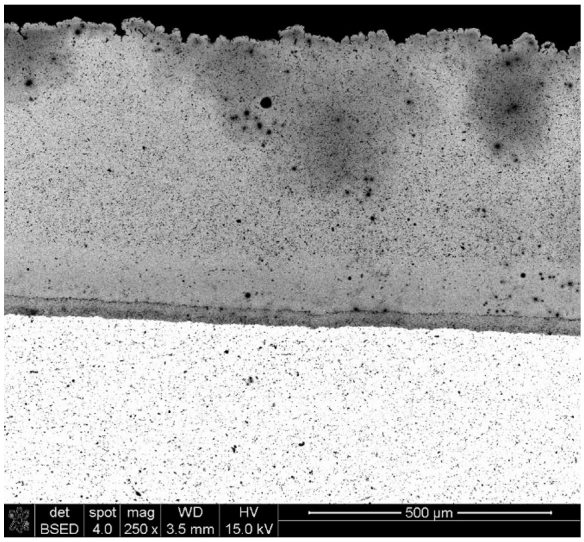

Figure 66: SEM micrograph of Round 2 bond coat after annealing

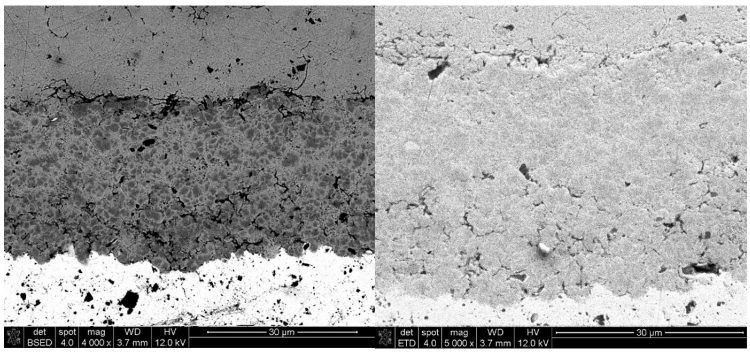

Figure 67: SEM images of Round 2 bond coat after annealing with significant cracking seen. Left: BSED detector and Right: ETD detector showing different contrast

The interface after annealing reveals a large amount of cracks at both interfaces of Nb/Nano Al-Trans and Nano Al-Trans/Cu. Due to CTE mismatch or thermal stress build-up during deposition, these cracks were formed during the annealing process. This directly explains the significant decrease of adhesion strength of samples containing a bond coat.

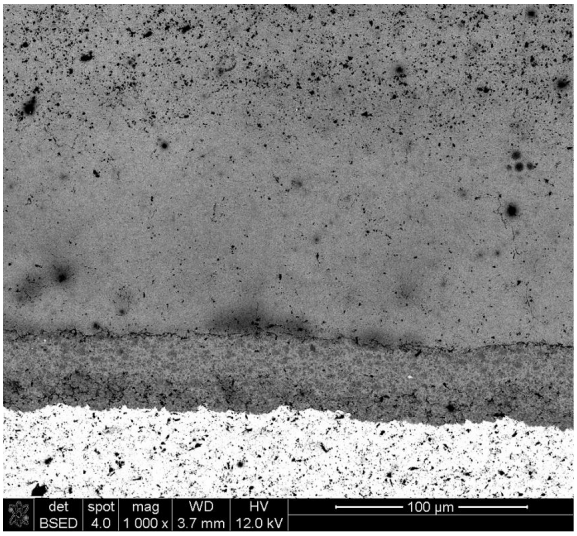

Figure 68: SEM image of Round 2 bond coat after annealing with 150μm layer of densification seen

Something interesting to see is the tamping effect of the samples consisting of a bond coat. These samples were not etched like other samples were. This is due to the bond coating containing Al and not knowing how the Cu etchant would effect this coating. A large area of tamping effect is seen in the micrograph above of 100-150μm. There is a layer of reduced porosity seen in the coating attributed from the tamping effect. This is larger than other coating. The reason for this could be attributed to the hardness of the substrate with Nano Al-Trans coating being a harder substrate than Nb. This can shed light onto the tamping effect seen between Round 1 and Round 2 previously discussed. Round 1 having a thicker layer of tamping correlates to the harder Nb substrate created from the B_4C abrasive media, whereas Round 2 utilizes SiC abrasive media to create a lesser increase in substrate hardness and thus less tamping effect. This suggests that hardness of substrate has a direct relationship on the amount of coating densification for given spray parameters.

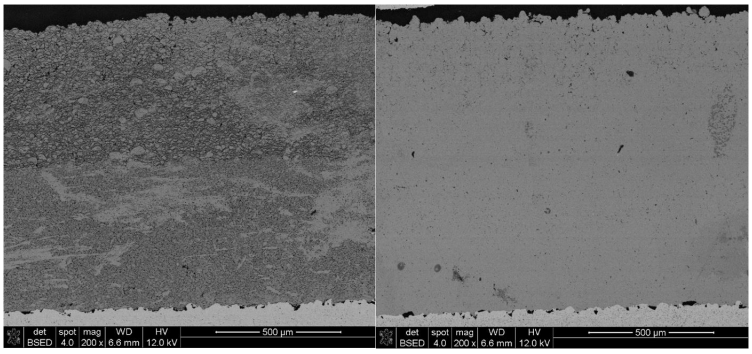

Figure 69: Before annealing: SEM images of Round 2 double coating

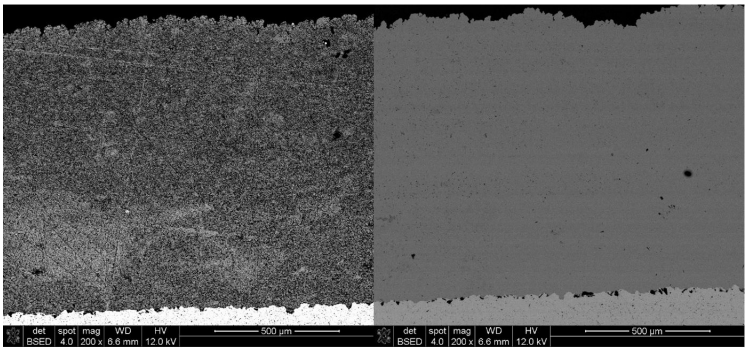

Figure 70: After annealing: SEM images of Round 2 double coating

A sample from Round 1 was leftover without a particular purpose. The sample consisted of a coating of 0.5mm and was annealed successfully. The sample was sprayed with a second coating in Round 2. This sample underwent no extra surface preparation of the previously deposited Cu coating. The images above show SEM cross sections of the double layer coating with BSED on the left and ETD on the right. The first layer is annealed in all images while the second layer has both before annealing and post annealing images. One takeaway here is that there remains porosity in the second coating before annealing. This is porosity of copper depositing on copper. Cu powder on Cu (Cu/Cu) substrate should be an easier spray combination that requires less velocity than the Cu/Nb spray pair. This further shows how not only is the surface preparation far from optimal, the spray parameters are also not optimal. Optimal spray parameters should excel at the deposition of Cu onto Cu and there should be significantly less porosity seen in the micrograph of the second layer.

4.6 Low Oxygen Copper

Powder samples were taken from Round 1 and Round 2 and ran through LECO testing. LECO testing is a method of determining the concentration of elements in a given metallic sample. This measurement determines the net concentration of an element, meaning that any oxygen content found represents the sum of surface oxides and internal oxides. Understanding the oxygen content of the powder used and of the sprayed samples can help explain results.

Table 10: LECO results of Round 1 and Round 2 from atomization to post-spray

Timeline of Measurements	Location	Round 1 Praxair - 2015 (ppm)	Round 2 Praxair - 2018 (ppm)
Post Atomization - Oxygen	Praxair via LECO	300	300
Pre Spray Powder - Oxygen	NCSU via LECO	941	511
Pre Spray Powder - Hydrogen	NCSU via LECO	12.6	9.4
Post Spray Sample - Oxygen	NCSU via LECO	1298	863
Post Spray Sample - Hydrogen	NCSU via LECO	18.1	7.84
Oxygen Pickup from Storage	-	641	211

The results followed what is suggested in literature. Oxygen content can reduce deposition quality as a higher velocity is needed to sufficiently break the surface oxides of the powder. Also, even as surface oxides are broken they can become entrapped as the subsequent powder builds up. Both rounds of spraying held the same estimated velocity of deposition. Based on what we know, the powder from Round 1 with higher oxygen content should require higher energy to create the same deposition as powder from Round 2 with lower oxygen content. This is another of multiple contributing factors to the failed adhesion in Round 1 and the large improvements made in Round 2.

Oxygen pickup was minimized through sieving, storing, and spraying with minimal exposure to air. It is currently difficult to completely mitigate oxygen pickup in Cu powder and most metal powders. For most powders it is not necessary to minimize oxygen content so the infrastructure for low-oxygen content powder has not been fully established. A customized setup that would allow for direct transfer from atomization to powder hopper would be ideal. This powder hopper could then be sieved and stored in an inert atmosphere. Then oxygen pickup could be mitigated through similar methods to ours of transferring containers and spraying in a quasi-inert atmosphere. This can be improved upon easily if needed. While there are multiple factors contributing to the improvement of results for Round 2, it corresponds to literature that a lower oxygen content allows for better deposition and should be considered for any subsequent deposition of Cu. This is particularly true if there is no metallurgical bond and the adhesion characteristics depend almost entirely on mechanical interlocking as in this study.

4.7 Complex Geometry

The long term application of this cold spray pair requires deposition onto complex geometries. In particular, the geometries in question are seen in the figure below with high curvature.

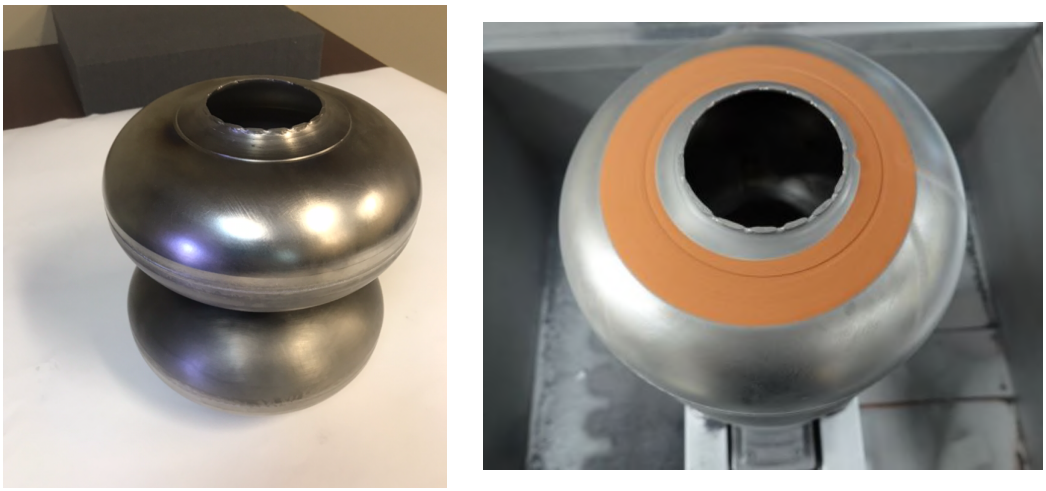

Figure 71: Spraying of complex geometry elliptical niobium SRF structure before cleaning (Left) and after spraying (Right)

In a more complete structure that may be longer or have a smaller diameter, the spray orientation might look more like a skewer with the part mounted horizontally. However, for this test piece the sample was mounted vertically as was the least intensive method. The structure was mounted with the intention of demonstrating an ability to execute a pre-programmed spray path. The spray path would be g-code generated through the software of Inovati and a CAD design of the structure in question. The area to be coated was towards the top of the elliptical structrue as seen in the images. The spray path chosen was a spiral beginning with a smaller diameter slowly increasing, the rotation velocity of the structure was reduced proportionally to maintain the same nozzle to surface translation speed. There are multiple ways to create this spray path and this is the execution of one of them. This may prove useful for other geometries if needed as well as a spray path designed to mitigate thermal stress build-up in the coating or the interface.

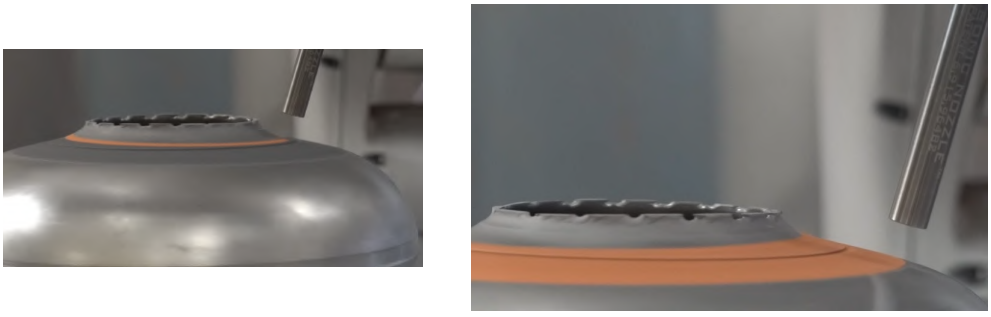

Figure 72: Spraying of complex geometry elliptical niobium SRF structure initial (Left) and final (Right)

The elliptical cavity was coated with Cu of thickness 0.2mm to prove the ability to deposit onto complex geometries. The coating adhered well although no adhesion testing will be done. This test piece

was more for a demonstration. The demonstration was a success and shows the future process of coating real structures with complex geometries as an achievable goal.

5 Conclusion

Superconducting radio frequency structures operate at cryogenic temperatures and are continuously optimized to increase efficiency and to be more cost effective. Optimization requires conservation of material properties and thus any optimization should be able to coincide with current processing techniques and operating environments as much as possible. Cold spray technology offers a unique solution as deposition is performed at temperatures that will not effect material properties and are able to fit in with common processing techniques. This study aims to determine the parameters required for effective deposition of copper onto niobium, primarily focused on adhesion, and whether this cold spray pair is capable of performing at common operating conditions.

Cu powder was deposited onto high purity Nb substrate via cold spray to understand the characteristics necessary for adhesion. The surface of the Nb substrate was grit blasted with different abrasive media in multiple trials and each sample was characterized to assess adhesion and potential for thermal efficiency across the Nb interface and the Cu coating.

It was found that effective deposition of this cold spray pair depends solely on mechanical interlocking as Cu and Nb have very limited solid solubility with vastly different melting temperatures. The spray pair does not allow for metallurgical bonding at the processing temperatures. The level of mechanical interlocking is found to be effected by substrate preparation and surface roughness, oxygen content of copper powder, particle velocity, gas temperature, and powder morphology and particle size distribution. The parameters of particle velocity, gas temperature, and powder morphology (SP) were held constant across trials and are sufficiently presented in literature as significant cold spray variables for deposition of Cu. This study explores multiple substrate preparation techniques with multiple batches of powder with varying oxygen content. We have demonstrated that good adhesion (48MPa) between the Nb substrate and Cu coating can be achieved. Thin, 0.6mm coatings remain adherent during 800°C thermal annealing with a resulting electrical conductivity of 89%IACS. Conductivity of cold spray copper coatings are found to recover significantly from 50%IACS to 89%IACS. Unfortunately, achieving this adhesion required SiC grit blasting to promote mechanical interlocking. Use of abrasive media resulted in strong embedding of media in the niobium substrate. Some alternative methods of providing surface roughness without the use of abrasive media were attempted without success or adhesion. While sufficient for mechanical purposes, this low conductivity media will have detrimental effects on the thermal interface conductivity of the conduction

cooled cavity. It was also found that minimizing oxygen pickup in copper powder is possible through proper handling techniques. Minimization of oxygen content in copper powder is worthwhile as reduced oxygen content can create higher quality coatings, corresponding to literature and reinforced in this study. Furthermore, we demonstrated that a robotically controlled cold spray process can coat the contour of elliptical-style cavities while maintaining proper incidence angle and standoff distance throughout.

This represents the first-known documented study on cold spray of copper onto niobium for the application of SRF structures. This serves as a reference for Cu/Nb spray for any future development and as an introduction of how cold spray can be applied to SRF accelerating structures. The existing literature on cold spray technology is summarized as well as an understanding of copper and niobium compatibility.

The study had limitations of scope changes and availability of resources. As the study advanced, scope changes were made to focus on achieving adhesion. The study originally prioritized a broad range of measurements and data as a preliminary test in determining the potential of this spray pair application. At the same time, RadiaBeam does not currently have the ability to test RRR samples, so samples were sent to Argonne National Lab. RRR measurements were significantly delayed and samples from this study are not going to be tested. These measurements would have been very interesting to include and offer a great baseline of cold sprayed copper behavior at cryogenic temperatures.

This project began without in-depth experience in cold spray technology and was completed in the span of 9 months with a significant development in the understanding of Cu/Nb cold spray. While the fundamentals of cold spray technology are relatively easy to grasp, understanding cold spray well enough to optimally combine dissimilar materials such as Cu/Nb that have not been sprayed as a pair before requires trial and error. This resulted in Round 1, applying general cold spray practices and developing parameters from this base and learning to establish improvements in Round 2. Alternative methods to grit blasting to eliminate embedding were unknown at the time of Round 1 deposition. This prompted some ideas for Round 2 of utilizing sand paper and turning samples which was unsuccessful. The main goal of Round 2 was to provide adhesion through changes in powder and substrate preparation without changing spray parameters such as pressure or temperature. The estimated velocity from pressure and temperature of both Round 1 and Round 2 were the same, a unanimous decision backed by collaborators. Some alternative methods discovered after the study involve spraying the coating material either above erosion velocity or at a large incidence angle to roughen the surface.

Low oxygen powder was utilized in this study but the extent of oxygen reduction was limited. Low oxygen was achieved through safe practices only available in-house. Access to powder starting directly after atomization would result in this oxygen content significantly reduced to even below 10 ppm. However, we were able to show a difference between the two powders proving that our method to reduce oxygen content

was successful and the reduction of oxygen content in powder increased coating quality. Through development of heat treatment and hydrogen degassing, the vacuum tube furnace used was not able to provide as much insight as ideal. The tube furnace was not leak checked and did not have an RGA attached for proper hydrogen and oxygen degassing analysis. Once samples were created, the porosity was qualitatively measured from SEM micrographs. This worked for the scope of the study. However, a more easily repeatable, non-destructive, and quantifiable measurement for porosity would be very useful.

5.1 Future Work

If this study is explored further by us or any other group, it is recommended to continue to explore low oxygen content copper powder. With a new wave of funding, contacting atomization company directly inquiring about eliminating powder exposure to air is the next step. This ties directly into RRR measurements as low oxygen content will stop showing significant differences between coatings at room temperature. However, oxygen content, densification, and porosity will have a large impact on RRR values. RRR measurements from ANL would be one of the first steps in any future work if we were to continue. RRR measurements should be considered by anyone continuing this work. However, if there is ample time then it is suggested to develop a better baseline for coatings before sending any samples for RRR.

Modifying spray parameters such as increasing pressure and particle velocity would be one of the first changes if a new round of samples were to be sprayed. A surface preparation technique that was not utilized was spraying copper powder above erosion velocity for an initial time period before spraying at desired deposition velocity. This technique is utilized for substrates that require surface roughness but consists of a material such that grit blasting causes significant embedding. Cu powder could also be sprayed at a large incidence angle to roughen the surface without adhesion and eliminating embedding. Using the coating material to roughen the surface either above erosion velocity or at a large incidence angle appears to be a very promising technique for the spray pair of copper powder and niobium substrate. Exploring the metallographic analysis at the interface through niobium etching would offer more insight on the effect of different surface preparation techniques. The microhardness of these areas of interest of the niobium near and at the interface as well as microhardness of all copper coatings before and after annealing would offer insight to surface preparation and deposition characteristics.

If a different cold spray system is used in the future such as high pressure CS, this study offers insight into comparing kinetic metallization with high pressure cold spray. It is entirely possible this cold spray pair behaves better under high pressure cold spray such as 1000m/s than the kinetic metallization used in this study at 700m/s. This study can be directly compared to highlight any possible differences found.

Finally, while the cold spray of copper on niobium is a relevant spray pair, it is not the only spray pair relevant to SRF structures. Establishing the need for mechanical stabilization of these structures is still worthwhile without the the thermal capabilities of copper. Cold spray of titanium onto niobium could offer a solution to mechanical stabilization of these structures.

References

[1] W. Singer. SC Cavities; Material, Fabrication, and QA, 2009.

[2] Robert Kephart. Conduction cooling systems for linear accelerator cavities. 5 2017.

[3] Robert Kephart. Srf, compact accelerators for industry society. *Proceedings of SRF2015, Whistler, BC, Canada*, 2015.

[4] H.S. Yang B.S. Lee Y.S. Choi, D.L. Kim and W.M. Jung. Cryocooled Cooling System for Superconducting Magnet. *Cryocoolers*, 15, 2009.

[5] S. Posen, M. Liepe, D. Hall. Proof-of-principle demonstration of nb3sn superconducting radiofrequency cavities for high q_0 applications. *Appl. Phys. Lett*, (106), 2015.

[6] Ray Radebaugh. Cryocoolers: the state of the art and recent developments. *Journal of Physics: Condensed Matter*, 21(16), 2009. doi: https://doi.org/10.1088/0953-8984/21/16/164219.

[7] Jayakar Charles Tobin Thangaraj. Compacy, high power SRF Accelerators for Industrial Applications, 2018.

[8] R. Kostin, A. Kanareykin, R.D. Kephart, J.C.T. Thangaraj, R.C. Dhuley, M.I. Geelhoed, T.K. Kroc. Operation regime analysis of conduction cooled cavities through multi-physics simulation. *JACoW Publishing*, 2018. doi: 10.18429/JACoW-IPAC2018-WEPML010.

[9] H. Padamsee. Design topics for superconducting rf cavities and ancillaries. *Cornell University*.

[10] Ram C. Dhuley, Roman Kostin. Thermal link design for conduction cooling of srf cavities using cryocoolers. *IEEE Transactions On Applied Superconductivity*, 29. doi: 10.1109/TASC.2019.2901252.

[11] Zachary Conway. Development of a Half-Wave Resonator Cryomodule for Ion Beams, 2015.

[12] Roman Gr. Maev, Volf Leshchynsky. 2016. ISBN 978-1-4665-8443-3.

[13] Arbegast Materials Processing and Joining Lab. Cold Spray A guide to best practice. Technical report, South Dakota School of Mines and Technology, 2012.

[14] Stephen Yue. Cold spray of copper. Technical report, Materials Engineering, McGill University, 2019.

[15] Harminder Singh. Cold spray technology: future of coating deposition processes. *Frattura ed Integrità Strutturale*, 22:199–84, 2012.

[16] Travis Crowe Ralph Tapphorn, Howard Gabel. Solid-state additive manufacturing. URL `https://www.inovati.com/index.php`.

[17] Christian A. Widener Ozan Ç. Özdemir. Gas dynamics of cold spray control of deposition. Technical report, Advanced Materials Processing and Joining Laboratory, South Dakota School of Mines and Technology, 2017. URL `https://www.sdsmt.edu/Research/Research-Laboratories/AMP/Research/Presentations/`.

[18] Frank Gartner Horst Richter Thorsten Stoltenhoff Heinrich Kreye Tobias Schmidt, Hamid Assadi and Thomas Klassen. From Particle Acceleration to Impact and Bonding in Cold Spraying. *Journal of Thermal Spray Technology*, 18:794–808, 2009. doi: http://dx.doi.org/10.1007/s11666-009-9357-7.

[19] P.H. Shipway T. Hussain, D.G. McCartney and D. Zhang. Bonding Mechanisms in Cold Spraying: The Contributions of Metallurgical and Mechanical Components. *Journal of Thermal Spray Technology*, 18(3), 2009. doi: https://doi.org/10.1007/s11666-009-9298-1.

[20] Hamid Assadi Heinrich Kreye Tobias Schmidt, Frank Gartner. Development of a generalized parameter window of cold spray deposition. *Acta Materiala*, 54:729–742, 2006. doi: https://doi.org/10.1016/j.actamat.2005.10.005.

[21] Olakanmi Eyitayo Els-Botes A. Kutua Said. Matsagopane, Gaamangwe. Conceptual Design Framework for Setting Up Aluminum Alloy Powder Production System for Selective Laser Melting (SLM) Process. *JOM*, 2019. doi: https://doi.org/10.1007/s11837-019-03431-w.

[22] Andrew Vackel. Residual stress in thermal spray coatings and its implications on coating-substrate fatigue life. URL `https://www.osti.gov/servlets/purl/1429422`.

[23] Pasquale Cavaliere, editor. Springer, 2018. doi: 10.1007/978-3-319-67183-3.

[24] N.M. Chavan S.V. Joshi S. Kumar, M. Ramakrishna. Correlation of splat state with deposition characteristics of cold sprayed niobium coatings. *Acta Materialia*, 130:177–195, 2017. doi: http://dx.doi.org/10.1016/j.actamat.2017.03.023.

[25] Thorsten Stoltenhoff Heinrich Kreye Hamid Assadi, Frank Gartner. Bonding mechanism in cold gas spraying. *Acta Materiala*, 51:4379–4394, 2003. doi: https://doi.org/10.1016/S1359-6454(03)00274-X.

[26] Wen-Ya Li Chang-Jiu Li. Deposition characteristics of titanium coating in cold spraying. *Surface and Coatings Technology*, 167:278–283, 2003. doi: https://doi.org/10.1016/S0257-8972(02)00919-2.

[27] S. I. Imbriglio. Failure dynamics of spherical and irregular shaped Ti splats deposited on sapphire by cold spray. *Surface Topography: Metrology and Properties*, 7, 2019. doi: https://doi.org/10.1088/2051-672X/ab3efc.

[28] Carpenter additive. URL `https://www.carpenteradditive.com/`.

[29] Christophe Verdy Hanlin Liao Zhongming Ren Sihao Deng Chaoyue Chen, Yingchun Xie. Numerical investigation of transient coating build-up and heat transfer in cold spray. *Surface Coatings and Technology*, 326:355–365, 2017. doi: https://doi.org/10.1016/j.surfcoat.2017.07.069.

[30] What is dissimilar metal welding? URL `https://www.spilasers.com/application-welding/dissimilar-metal-welding-definition/`.

[31] Mario Guagliano Ramin Ghelichi. Coating by the Cold Spray Process: a state of the art. *Frattura ed Integrità Strutturale*, 8:30–44, 2009. doi: https://doi.org/10.3221/IGF-ESIS.08.03.

[32] Changhee Lee S. Kumar, Gyuyeol Bae. Influence of substrate roughness on bonding mechanism in cold spray. *Surface and Coatings Technology*, 304:592–605, 2016. doi: http://dx.doi.org/10.1016/j.surfcoat.2016.07.082.

[33] R. Fernandez T. Samson, D. MacDonald and B. Jodoin. Effect of Pulsed Waterjet Surface Preparation on the Adhesion Strength of Cold Gas Dynamic Sprayed Aluminum Coatings. *Journal of Thermal Spray Technology*, 24(6), 2015. doi: https://doi.org/10.1007/s11666-015-0261-z.

[34] H. Misran T. Okabe A. Manap, O. Nooririnah and K. Ogawa. Experimental and SPH study of cold spray impact between similar and dissimilar metals. *Surface Engineering*, 30(5), 2014. doi: https://doi.org/10.1179/1743294413Y.0000000237.

[35] Adrian R. Wagner. Diffusion Bonding of Copper to Niobium. Master's thesis, 2015.

[36] K. SCHULZE O. F. DE LIMA, M. KREHL. Wetting characteristics of copper on niobium. *Journal of Materials Science*, 20:2464–2470, 1985. doi: https://doi.org/10.1007/BF00556075.

[37] H. Okamoto. Cu-Nb (Copper-Niobium). *Journal of Phase Equilibria and Diffusion*, 33(4):344, 2012. doi: https://doi.org/10.1007/s11669-012-0051-y.

[38] J.D. Fuerst. Niobium to Stainless Steel Braze Transition Development.

[39] S. Mandal Vahid Tari, Ben Anglin and A.D. Rollett. Transformation Texture and Orientation Relationship, 2016.

[40] H.M. Rosenberg. The Thermal Conductivity of Metals at Low Temperatures. *Philosophical Transactions of the Royal Society of London. Series A, Mathematical and Physical Sciences*, 247(933): 441–497, 1955.

[41] A. McGinnis. Residual stresses in a multilayer system of coatings. *Adcances in X-Ray Analysis*, 1999.

[42] Hanlin Liaoc Wen-Ya Li, Chang-Jiu Li. Significant influence of particle surface oxidation on deposition efficiency, interface microstructure and adhesive strength of cold-sprayed copper coatings. *Applied Surface Science*, 256:4953–4958, 2010. doi: https://doi.org/10.1016/j.apsusc.2010.03.008.

[43] Kairet Thomas. *A contribution to the study of cold gas dynamic spraying of copper: Influence of the powder characteristics on the mechanical properties of the coating* . PhD thesis, 2007.

[44] William J. Marple. The Cold Gas-Dynamic Spray and Characterization of Microcrystalline and Nanocrystalline Copper Alloys. Master's thesis, 2012.

[45] Antoine, C. Materials and surface aspects in the development of srf niobium cavities. 8 2012. URL `http://cern.ch/eucard`.

[46] G.S. Lodhab K.J.S. Sokheya, S.K. Raib. Oxidation studies of niobium thin films at room temperature by X-ray reflectivity. *Applied Surface Science*, 257:222–226, 2010. doi: https://doi.org/10.1016/j.apsusc.2010.06.069.

[47] R.E. Reed-Hill J.R. Donoso. Slow Strain-Rate Embrittlement of Niobium by Oxygen. *Metallurgical Transactions A*, 7A:961–965, 1976.

[48] P. Duthil. Materials properties at low temperatures, 2013.

[49] S. Prat M. Fouaidy, N. Hammoudi. RRR of Copper Coating and Low Temperature Electrical Resistivity of Material for TTF Couplers, 2003.

[50] Table of iacs conductivities. URL `https://wwww.ihiconnectors.com/IACS-conductivity-electrical-alloys.html`.

[51] The wiedemann-franz law. URL `http://hyperphysics.phy-astr.gsu.edu/hbase/thermo/thercond.html`.

[52] G.F. Vander Voort. *Metallography, principles and practice*. ASM International, 1999.